Ollscoil na hÉireann, Corcaigh

National University of Ireland, Cork

University College Cork, Ireland
Coláiste na hOllscoile Corcaigh

A Drifter-based Self-powered Piezoelectric Sensor for Ocean Wave Measurements

Thesis presented by

Seyyed Masoud Kargar

for the degree of

MEngSc (Research) - Mechanical Engineering

University College Cork

School of Engineering and Architecture - Electrical and Electronic Engineering

Head of School/Department: Prof. Jorge Oliveira

Supervisor(s): Dr. Guangbo Hao, Dr. Richard Kavanagh

July 2022

Table of Contents

Declaration

I hereby declare that this submission is my work and that, to the best of my knowledge and belief, it contains no material previously published or written by another person or material that has to a substantial extent been accepted for the award of any other degree or diploma at any university or other institution of higher learning, except where due acknowledgment has been made in the text.

Acknowledgements

First and foremost, I would like to take the opportunity to thank my supervisor, teacher, and friend, Dr. Guangbo Hao, who has provided me with the opportunity to be a Research Master's student at University College Cork. I deeply appreciate all the time he has dedicated to teaching me not only the way of research but also the way of life. His patience in supervision and his commitment to supporting his students in their lives as well as their research are among his most astonishing attributes. I thank him for all his support during my time at University College Cork.

I am grateful to my co-supervisor, prof. Richard Kavanagh, for his guidance and support during my project.

I would also like to thank Mr. TJ Horgan, the project manager, for all his support and for providing the funding opportunity for my research at University College Cork.

My heartfelt gratitude and best wishes go to my wife Mehrnaz for her patience, love, and care, as well as to my parents Seyyed Jabbar and Zahra, for all their love and sacrifice in bringing me to this point in my life.

Finally, I appreciate the SELKIE for awarding a full scholarship for my studies as a research master's at University College Cork.

List of Publications

1) Seyyed Masoud Kargar, Guangbo Hao. 2022"An Atlas of Piezoelectric Energy Harvesters in Oceanic Applications", Sensors (Q1, IF: 3.576) https://doi.org/10.3390/s22051949
2) Seyyed Masoud Kargar, Guangbo Hao. 2022"A Drifter-based Self-powered Piezoelectric Sensor for Ocean Wave Measurements", Sensors (Q1, IF: 3.576), (Invited Paper), https://doi.org/10.3390/s22135050

Abstract

In the present research, a drifter-based piezoelectric sensor is proposed to measure ocean waves' height and period. To analyze the motion principle and the working performance of the proposed drifter-based piezoelectric sensor, a dynamic model is developed. The developed dynamic model investigates the system's response to an input of ocean waves and provides design insights into the geometrical and material parameters. Next, finite element analysis (FEA) simulations using the commercial software COMSOL-Multiphysics have been carried out with the help of a coupled physics analysis of Solid Mechanics and Electrostatics Modules to achieve the output voltages. An experimental prototype has been fabricated and tested to validate the results of the dynamic model and the FEA simulation. A slider-crank mechanism is used to mimic ocean waves throughout the experiment, and the results show a close match between the proposed dynamic modeling, FEA simulations, and experimental testing. In the end, a short discussion is devoted to interpreting the output results; comparing the results of the simulations and the experimental testing; the sensor's resolution; and the self-powering functionality of the proposed drifter-based piezoelectric sensor.

List of Figures

List of Tables

Abbreviation and Acronyms

PZT	Lead Zirconate Titanate
PVDF	Polyvinylidene Fluoride
MFC	Macro-Fiber Composites
VIV	Vortex-Induced Vibrations
SEV	Self-Excited Vibrations
ADCP	Acoustic Doppler Current Profilers
PVC	Polyvinyl Chloride
FEA	Finite Element Analysis
PC	Personal Computer
AC	Alternative Current
DC	Direct Current

Nomenclature

D	Electrical Displacement
d	Piezoelectric Coefficient
T	Stress
ε	Permittivity
E	Electric Field
X	Strain
s	Mechanical Compliance
d_{ij}	The ratio of the Strain to the Electric Field
M_p	Mass of the Piezoelectric
K_p	Stiffness of the Piezoelectric
Y_p	Displacement of the Piezoelectric
C_p	Damping Coefficient of the Piezoelectric
M_d	Mass of the Drifter
K_d	Stiffness of the Drifter
Y_d	Displacement of the Drifter
Y_w	The motion of the Ocean Waves
F_{i1}	The Piezoelectric Disk's Inertial Force
F_{i2}	The Drifter's Inertial Force
F_{e1}	The Piezoelectric Disk's Elastic Force
F_{e2}	The Drifter's Elastic Force
F_{d1}	The Piezoelectric Disk's Damping Force
V	Voltage
Q	Charge

C	The capacitance of the Piezoelectric Disk
F	Force
ε_r	Relative Permittivity
ε_0	Vacuum Permittivity
A	Area
t	Thickness
ρ	Density
v	Volume
E	Young's Modulus
l	Length of the Material
H	Wave's Height
V_{out}	Maximum Output Voltage
P	Power
R	Resistance
T	Period

1. Introduction and Background

1.1 Introduction

Being harsh, the marine environment requires regular and real-time measurements. There are lots of facilities and sites throughout the oceans, and it is of high significance to prevent any possible damage to them due to the ocean's powerful and impactful waves. Therefore, sensors are required to measure oceanic waves to predict their power and reduce the risk of damage to oceanic facilities and sites. [1]

Currently, oceanic waves are monitored by several techniques such as buoys, micro-seism analysis, coastal radars, and satellite observations. Each of the techniques has its limitations. For example, having a long anchor in buoys causes problems for fishing in the oceans. Moreover, they contain sensitive devices that can be easily damaged. In the case of radar sensors, they show a low signal-to-noise ratio, which limits the accuracy of detecting lower wave heights. Satellite sensors also show imperfect radiometric, spatial, and spectral resolutions. [2]

After the introduction of piezoelectricity [3], piezoelectric materials have gained considerable attention in research and industry over time. Employing direct and converse piezoelectric effects, piezoelectric materials are utilized in various applications as sensors, actuators, and energy harvesters. [4]

Taking advantage of the direct piezoelectric effect, different piezoelectric-based sensors are designed for pressure and stress [5-7], acceleration [8-10], tactile [11, 12], medical diagnostics [13, 14], acoustics [15], structural health monitoring [16], etc. Moreover, using the same principle, many energy harvesters have been designed based on the piezoelectric principle for different applications, such as in transportation [17], wearable electronics [18], microfluidics [19], wind and ocean energies [20, 21], and biomedical engineering [22].

Piezoelectric materials started to be used in the ocean as an energy harvester in the 1970s. After that, numerous piezoelectric energy harvesters have been designed for oceanic applications. In the present research, using the same principle as in piezoelectric energy harvesters, a drifter-based piezoelectric sensor is proposed to measure oceanic waves' height and period, which has the following advantages:

- Capable of being self-powered;
- Providing real-time measurement;
- Accurately measure oceanic waves, even those of very small magnitude;
- Precisely measure the waves' period; and
- Have a simple but robust structure.

The rest of this chapter elaborates on the fundamental concepts of this research, such as piezoelectricity, piezoelectric energy harvesters, oceanic drifters, ocean waves, and the location of the facilities in the oceans to help the reader follow the content of it. Then, the research motivation, objectives, and thesis layout will be discussed.

1.2 Piezoelectricity

In 1880, the term piezoelectricity was introduced by brothers Pierre and Jacques Curie [3], which has been intensively studied in recent years for different sensory and actuation applications in different fields. Later, in 1881, the brothers Curie validated their work on the inverse piezoelectric effect with experiments [23]. Stressing a piezoelectric material would result in a change in its atomic configuration, which forms dipole moments. This phenomenon is called the direct piezoelectric effect, in which the piezoelectric material generates electricity as a reaction to the applied force. Therefore, if a periodic force (tension or compression) is applied to the material, an alternative current (AC) voltage will be the output. On the other hand, if the piezoelectric material is electrically polarized, the converse piezoelectric effect appears in which the piezoelectric material extends/contracts as a result of the applied electrical voltage. It should be noted that in the inverse piezoelectric effect, lengthening or shortening of the piezoelectric material depends on the polarity and the applied poling voltage and can be reversed if the voltage direction is reversed [4]. Both the direct and converse effects of piezoelectricity are shown in Figure 1.1.

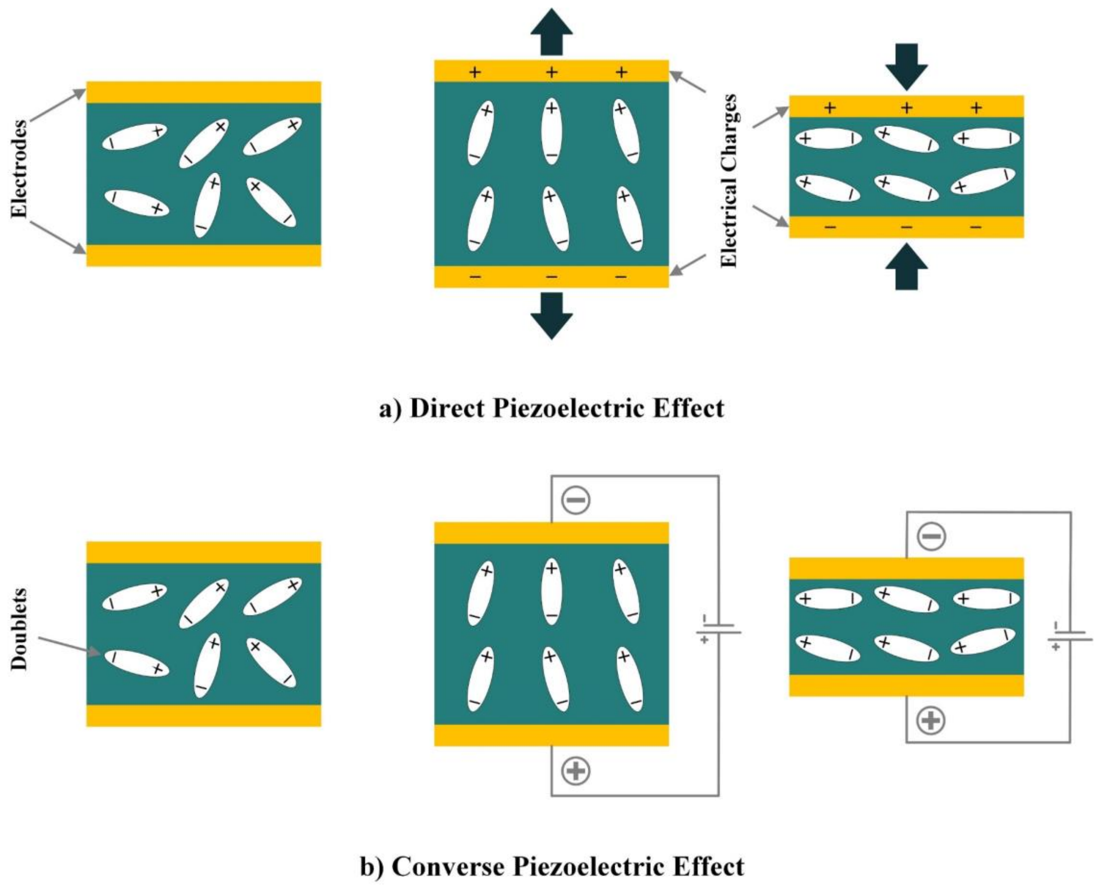

Figure 1. 1. Piezoelectric Effect; (a) Direct Piezoelectric Effect; (b) Converse Piezoelectric Effect.

There are many diverse applications for both direct and inverse piezoelectric effects, where the direct effect is utilized in the case of sensors and energy harvesters, and the inverse effect is used in actuators. These effects are governed by piezoelectric constitutive equations as [24]:

$$D = dT + \varepsilon E \tag{1.1}$$

$$X = sT + dE \tag{2.1}$$

where D, d, T, ε, E, X, and s, represent electrical displacement, piezoelectric coefficient, stress, the permittivity of the material, electric field, strain, and mechanical compliance, respectively.

1.3 Oceanic Piezoelectric Energy Harvesters

Mechanical energy, as one of the ambient sources of energy, can be converted into electrical energy by making use of different techniques. One of the most promising techniques to capture and convert mechanical energy is piezoelectric energy harvesters. Unlike electrostatic, electromagnetic, and triboelectric energy harvesters, which require another source of voltage, magnetic field, or contact with other materials, respectively, piezoelectric energy harvesters convert mechanical energy to electricity based on their intrinsic polarization [24].

Among different small-scale energy harvesters, piezoelectric materials show a considerable energy generation density that is about three times higher than the others [25]. Moreover, these materials can be simply attached to the systems, and as they contain no moving parts, they are free from frequent upkeep. Moreover, they have the merits of direct conversion of mechanical energy to electricity, being compact, structurally simple, clean, light-weight, stable, and very sensitive to any small strains. Although the generated electricity by piezoelectric energy harvesters is rather small, it is enough for low-energy-consumption electronics, such as oceanic sensors [23].

Oceanic piezoelectric energy harvesters employ water current, wave motion, and wave impact forces to extract energy from the ocean and convert it to usable electrical energy to power sensors and some other measurement devices [4]. These sources are very promising and available at all times during the day. Moreover, these energy sources in marine environments have a high density compared to the other sources of renewable energies, such as wind or solar energy [26].

1.3.1 Piezoelectric Materials

Active materials that can generate electricity as a reaction to small mechanical stress are called piezoelectric materials. The type of material for energy harvesting applications is of high importance to the performance and functionality of the harvester. Researchers have investigated numerous types of materials, such as organic, inorganic, composite, and bio-inspired materials, for piezoelectric energy harvesters [24]. Among them, PZT and PVDF are the most widely used materials for energy harvesting in oceanic applications. PZT, which is also known as Lead Zirconate Titanate, is a poled ferroelectric ceramic with the highest frequency of applications in piezoelectric energy harvesters. Even though PZT is one of the major materials in energy harvesting, its drawbacks, such as its drastic brittle nature and fatigue growth possibility in high-frequency loadings, limit its widespread usage in energy harvesting. On the other hand, to overcome the demerits of PZT, PVDF, also known as polyvinylidene fluoride, has been developed to improve the efficiency of piezoelectric energy harvesters [27]. Although PZT can produce more electricity when subjected to the same stress as PVDF, unlike PVDF, it cannot withstand high stress. PVDF shows a higher tensile strength value, which is about 2.6 times higher than PZT’s strength value [4]. The low stiffness, large tensile strength, and high flexibility of PVDF make it a unique choice for many applications, specifically in ocean energy harvesters. Apart from PZT and PVDF, macro-fiber composites (MFC) are also used in some of the literature in oceanic applications, which show great performance in energy harvesting from the ocean.

1.3.2 Coupling Modes

Piezoelectric materials present a kind of flexibility in their configurations, which makes them unique in energy harvesting applications. Based on the desired configuration in a particular application, piezoelectric materials' configurations can be altered by changing their electrode pattern, poling direction, and strain direction. Moreover, to tune the resonant frequency between the material and the energy source, volume and layers can be changed, and a pre-load force can be added [28].

The piezoelectric coefficient (d_{ij}) is the ratio of the strain to the electric field, where i denotes the direction of the polarity and j represents the mechanical stress direction. Figure 1.2 shows piezoelectric material axes for polarization as well as stress/strain. According to [29], d_{14}, d_{15}, d_{33}, and d_{31}, or simply 1-4, 1-5, 3-3, and 3-1, respectively, are the piezoelectric energy harvesters' configurations in oceanic applications. However, due to the complex configurations of 1-4 and 1-5 modes, they are less used in oceanic applications compared to 3-3 and 3-1 modes. Figure 1.3 shows the most utilized configurations, 3-3 and 3-1, in ocean applications. In the 3-3 mode, both the polarity and the mechanical stress are in the same direction, parallel to each other. However, in the case of 3-1, the direction of the mechanical stress is perpendicular to that of polarity [30]. It should also be noted that choosing the right configuration for designing a high-performance piezoelectric energy harvester plays a crucial role and thus should be carefully considered based on the design requirements.

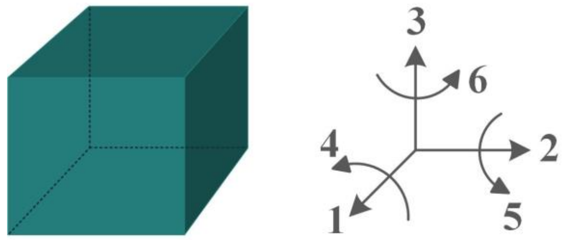

Figure 1. 2. Polarization axes of piezoelectric materials.

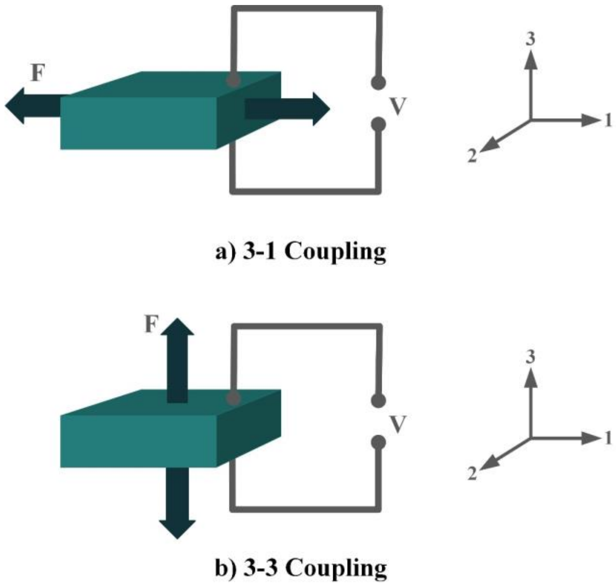

Figure 1. 3. Piezoelectric Coupling Modes; (**a**) 3-1 Coupling Mode; (**b**) 3-3 Coupling Mode.

1.3.3 Classification Based on Device Structure

The most common structure for a piezoelectric energy harvesting device is the cantilever beam configuration. This type of harvester employs one or two piezoelectric layers and is called unimorph and bimorph, respectively. Figure 1.4 shows cantilever beam structures with one and two layers of piezoelectric materials. As can be seen in Figure 1.4, piezoelectric layers are mostly bonded to a metallic non-piezoelectric material that is fixed at one end and acts as a flexural structure. As it is clear, taking advantage of two layers of piezoelectric materials, bimorph-type cantilever beams are capable of generating more output power compared to unimorph configurations. Therefore, bimorph configurations are found with a high frequency of applications in piezoelectric energy harvesters [31, 32].

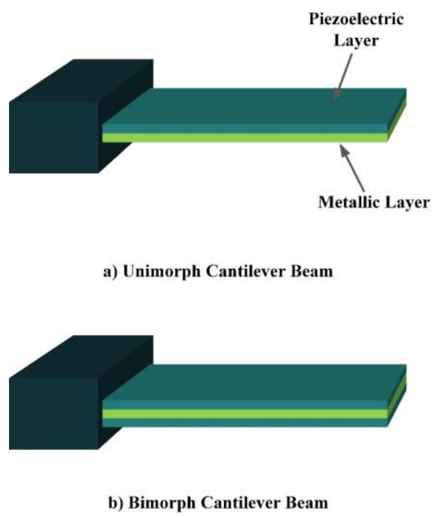

Figure 1. 4. Cantilever Beam Configuration; (**a**) Unimorph; (**b**) Bimorph.

The cantilever beam configuration utilizes the 3-1 coupling mode most often. However, there are designs in the literature that have used 3-3 coupling modes for cantilever structures, making use of interdigitated electrode designs. Moreover, it is usual to add a proof mass at the free end of the cantilever beam to tune the resonant frequency of the harvester with the environment [24].

The other configuration, which consists of a piezoelectric layer with a mostly disk shape, is the diaphragm structure. The piezoelectric layer is bonded to a metal shim. In some configurations, to improve functionality under low frequencies and to add a pre-loading unit to the energy harvester, a proof mass is attached to the diaphragm's core (Figure 1.5) [33].

Figure 1. 5. Diaphragm Configuration.

Adding two metallic endcaps in the shape of a cymbal on both sides of a piezoelectric disk would result in a new configuration called the cymbal structure (Figure 1.6). This configuration is indeed used to improve piezoelectric endurance when it is subjected to higher loads and impact forces. Moreover, the cymbal shape of the endcaps acts as a mechanical amplification unit due to the presence of the cavity in the center [33].

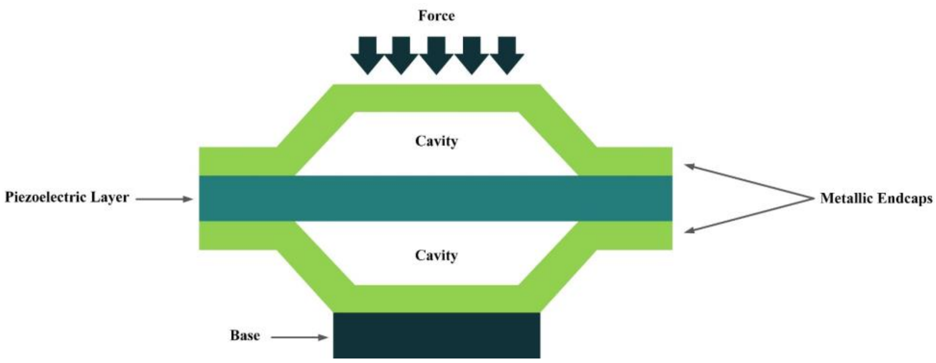

Figure 1. 6. Cymbal Configuration.

In addition to the other configurations, stacked piezoelectric structures can bear higher pressures. This configuration is made up of multiple layers of piezoelectric material stacked on top of each other. The poling direction of this type should be aligned with the applied force direction, as shown in Figure 1.7 [32].

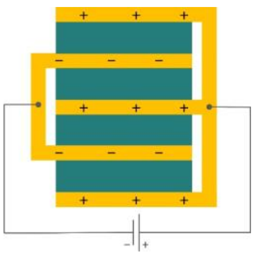

Figure 1. 7. Stacked Configuration.

All the aforementioned configurations have their merits and drawbacks. Each of them may be suitable for numerous applications and unsuitable for many others. Therefore, before employing one of them in an application, their limitations should be carefully studied and considered. In addition to the cantilever beam configuration's advantages, such as simple structure, low price, suitability for low-frequency applications, and higher mechanical quality factor, they are not able to withstand high impact forces. On the other hand, the cymbal configuration can bear impact forces and provide high energy output. However, the loss of mechanical input energy and being limited to applications requiring high vibration sources are its drawbacks. The circular diaphragm configuration is capable of working in pressure mode operations, but in a vibration mode application, it requires higher resonance frequencies. The stacked configuration is also suitable for working in pressure mode. It can also bear higher mechanical forces and provide higher outputs in the d_{33} coupling mode. Nevertheless, its high stiffness is among the challenges that should be addressed in the search for a proper application for it [33].

1.3.4 Ocean Energy Sources for Piezoelectric Energy Harvesters

Marine renewable energies are the source of many different energy converters [34, 35]. In the case of piezoelectric energy harvesters, water current, wave motion, and wave impact forces have been employed to extract energy from the ocean and convert it to usable electrical energy to power sensors and some other measurement devices [4]. These sources are very promising and available at all times during the day. Moreover, these energy sources in marine environments have a high density compared to the other sources of renewable energies, such as wind or solar energy [26]. In the following, a short introduction will be given to each of the marine energy sources that piezoelectric energy harvesters are designed for.

1.3.4.1 Water Currents

To employ piezoelectric energy harvesters to extract power from ocean water currents, the vibration in the water can be converted to electricity. To do so, the piezoelectric energy harvester should be placed in the current stream and be coupled with flow-induced vibration. Vortex-Induced Vibrations (VIV) and Self-Excited Vibrations (SEV) are the two significant flow-induced vibrations that are exploited by piezoelectric energy harvesters [36, 37].

To create VIV, a bluff body is located in a water stream, and depending on the characteristics of the bluff body, vortices of a particular size and frequency appear. If then, the piezoelectric energy harvester is placed behind the body, the generated vortices make it oscillate. This oscillation will generate electricity based on the piezoelectric principle [36].

Through the use of self-excitation of flexible bodies, here most often PVDF materials, SEV-based energy harvesting can be achieved. The bodies are placed in the flow stream and, with a minute increase in flow speed, the body attains self-excitation, which can be further used for electrical energy generation [37].

1.3.4.2 Wave Motion

Unlike water currents, where the energy is distributed all along, the waves' energy density diminishes by the depth and is concentrated near the surface of the ocean. Therefore, the facility's tip that captures the wave's energy should be close to the surface of the ocean [38]. According to [4, 39], piezoelectric energy harvesters from wave motion mainly consist of heaving and pitching bodies; the PVDF layer on the surface of the ocean; and fixed bodies on the ocean bottom.

1.3.4.3 Wave Impact

Another feature of the ocean is the impact of the waves on the ocean structure [39]. Mostly, wave impacts are considered destructive forces. However, these waves' forces on the structures can be advantageous rather than devastating. In the case that the piezoelectric energy harvesters are placed on the surfaces that are subjected to waves' impact, they can convert the applied pressure to electricity [4].

1.4 Oceanic Drifters (Drifting Buoys)

A drifter is a floating oceanographic device that is used to carry different measurement instruments for physical and biological oceanography. Transported by ocean currents and waves, drifters are also used to map flow patterns [40]. As they do not have any actuators for movement, they are classified as passive devices. Ocean waves and currents are the main drivers of the drifters [41].

Owning the merits such as being versatile and easily deployable at a low-cost, drifters have a considerable application in search and rescue operations, climate studies, and oil spill tracking in oceans. These devices in near-shore and off-shore deployments use GSM-based and satellite-based techniques for communication [42]. Figure 1.8 shows an example of a drifter that is used to carry a kinetic energy harvester in the ocean.

Figure 1. 8. An Example of Oceanic Drifters by Carandell et al. [42]

1.5 Ocean Waves

Waves in the oceans are generated by the association of forces, such as wind, atmospheric pressure gradients, earthquakes, gravitational attraction, and storms. Each of these waves is being restored and compensated by surface tension, gravity, and Coriolis force. Based on their periods, waves can be classified into seven groups: (1) Capillary waves; (2) Ultra-gravity waves; (3) Gravity waves; (4) Infra-gravity waves; (5) Long-period waves; (6) Ordinary tidal waves; and (7) Trans-tidal waves [43].

Capillary waves, ultra-gravity waves, and gravity waves are generated by wind force and restored by surface tension, surface tension and gravity, and gravity, respectively. Among them, capillary waves have the shortest period, which is less than 0.1 s. Ultra-gravity and gravity waves have a period of 0.1-1 s and 1-20 s, respectively. Infra-gravity waves last for 20 s to 5 min and are generated by wind and atmospheric pressure gradients. Gravity is the restoring force for this type of wave. Generated by atmospheric pressure gradients and earthquakes, long-period waves last longer than infra-gravity waves (about 5 min to 12 h) and are compensated by gravity. Ordinary tidal waves and trans-tidal waves have the longest periods among different types of waves, which are 12-24 h and more than 24 h, respectively. While ordinary tidal waves are generated by gravitational attraction, trans-tidal waves are generated by the combination of storms and gravitational attractions. Both of these waves are being compensated by gravity and Coriolis force. [43]

In general, there are two main factors in determining how much energy a wave holds (Figure 1.9): wave height and the wave’s period [44], meaning the time taken for a wave crest to travel the distance between two waves crests. Waves with a greater height and shorter periods contain more energy. However, unlike water currents where the energy is distributed all along, the waves’ energy density diminishes by the depth and is concentrated near the surface of the ocean. Therefore, the facility's tip that captures the wave's energy should be close to the surface of the ocean [38].

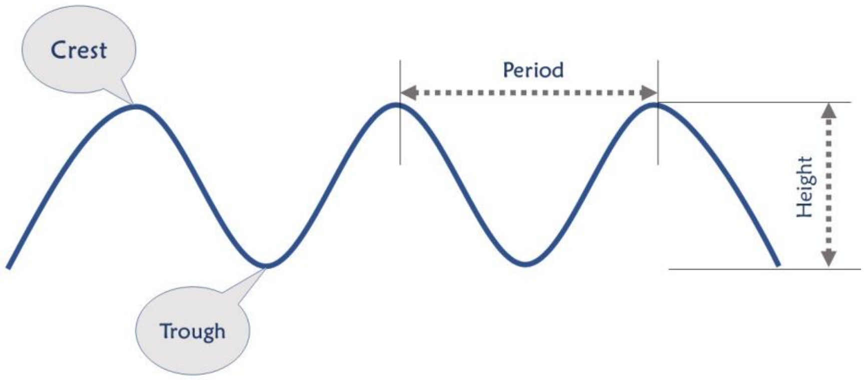

Figure 1. 9. Characteristics of an Oceanic Wave.

1.6 Location

Based on where the marine facilities are working, they can be categorized into three groups; onshore; nearshore; and offshore. Onshore represents regions with 10–15 m of water depth, where this value is 15–25 m for nearshore and is higher than 50 m for offshore. Figure 1.10 shows the different regions of the ocean [45].

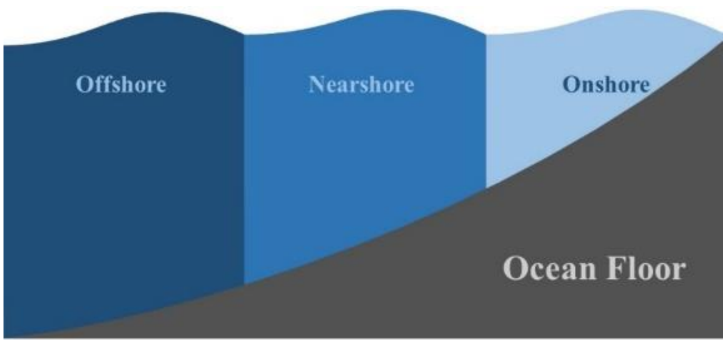

Figure 1. 10. Ocean Regions.

1.7 Motivations

The main motivations of the present research are as follows:

1) Considerable excellent state-of-the-art surveys have been provided in the field of piezoelectric energy harvesters and oceanic piezoelectric energy harvesters [4, 28, 29, 46]. However, as the number of designs is increasing rapidly, developing an atlas of the former designs seems necessary to help future researchers come up with their energy harvesters for oceanic applications.
2) Although there are various designs of piezoelectric energy harvesters for marine applications [47], piezoelectric materials have not been employed for sea and ocean wave measurements.
3) Conventionally, oceanic measurement devices have been powered by chemical batteries. However, most often, the life of the batteries is shorter than the life of the sensors. Therefore, the batteries require replacement or recharge, and both of these actions are very pricy, time-consuming, and laborious. Moreover, as batteries are bulky and heavy, they hinder the development of miniature, as well as light, electronic devices. On the other hand, the possibility of polluting the environment by the leaking of the dangerous chemicals inside batteries during replacement or recharge actions threatens oceans and the animals living in them. Therefore, it is of high importance to develop self-powered and self-chargeable devices for oceanic measurements. [23, 48]
4) Different types of sensory devices are utilized for ocean waves measurements [2]. However, almost all of these devices owning complex structure and high application costs. Therefore, developing a simple but robust structure that can measure ocean waves with high accuracy and resolution is necessary.

1.8 Thesis Aims and Layout

1.8.1 Objectives

Considering the disadvantages of the former ocean wave measurement devices, piezoelectric materials are selected in this research to address these shortages. Throughout this research, direct piezoelectric effect is used to demonstrate a self-powered piezoelectric sensor.

An atlas of 85 oceanic piezoelectric energy harvesters that have recently been reported in the state-of-the-art will be first provided with detailed information on their configurations, material, coupling modes, location, and power range. Then, a set of unified schematics will be drawn to show their working principles in this atlas. Stages of the design will be provided along with the working principle of the proposed sensor. Based Newton’s second law of motion, a dynamic model will be utilized to analyze the motion principle and the working performance of the proposed sensor. The proposed dynamic model will be simulated by taking advantage of the MATLAB/Simulink module. Finite element analysis using COMSOL Multiphysics will also be adopted to verify the results of the proposed dynamic model. In addition, an experimental prototype will be fabricated and tested to validate the results of the dynamic model and the FEA simulation. Finally, discussions will be provided on interpreting the output results; comparing the results of the simulations with those of the experimental testing; sensor’s resolution; and the self-powering functionality of the proposed drifter-based piezoelectric sensor.

1.8.2 Layout

The rest of this thesis is organized as follows:

Part of Chapter 2 is dedicated to reviewing the present techniques of ocean wave measurements and their working principles. Moreover, their merits and demerits are also investigated. On the other hand, as the present research investigates the feasibility of piezoelectric materials for oceanic wave measurements, the other part of Chapter 2 reviews the literature on piezoelectric materials in the oceans, which are almost exclusively used for energy harvesting from the oceans.

In Chapter 3, the configuration of the proposed sensor as well as its working principle are discussed and illustrated in detail.

In Chapter 4, the motion principle and the working performance of the proposed drifter-based piezoelectric sensor are analyzed using a dynamic model. Moreover, taking advantage of the commercial software COMSOL-Multiphysics, finite element analysis (FEA) has been carried out to verify the results of the proposed dynamic model.

Chapter 5 is dedicated to the prototype fabrication and testing of it to verify the results of the developed dynamic and FEA models.

Chapter 6 is dedicated to: 1) interpreting the output voltages; 2) comparing the three results coming out of the dynamic model, FEA simulation, and experimental testing; 3) investigating the resolution of the sensor to see the smallest wave that it can measure; and 4) the self-powering functionality of the sensor.

Chapter 7 provides a conclusion of the research and discusses future work.

2. Literature Review

As a natural phenomenon, oceanic waves have a significant influence on human activities. Therefore, monitoring this natural phenomenon is of high importance for our ocean-related activities such as meteorology, the safety of coastal areas, oceanic energy conversion, and navigation [2].

At the moment, oceanic waves are being monitored using techniques like buoys, micro-seism analysis, coastal radars, and satellite observations. Part of this chapter is dedicated to reviewing these techniques and their measurement principles. Moreover, their merits and demerits are also investigated.

On the other hand, the present research investigates the feasibility of piezoelectric materials for oceanic wave measurements. Therefore, the other part of this chapter reviews the literature on piezoelectric materials in the oceans, which are almost exclusively used for energy harvesting from the oceans. Moreover, to the best of the author's knowledge, although there are ample designs of piezoelectric energy harvesters in oceanic applications, piezoelectric material has not been employed for sea and ocean wave measurements.

2.1 Oceanic Waves Measurement Devices

Over the past decades, many important advances have been reported in the development of devices to measure oceanic waves, some of which are now available for measurement purposes based on various principles. In the following, several measurement techniques are outlined and their configuration, as well as working principles, are briefly discussed.

2.1.1 Wave Buoys

Buoys are a type of oceanic measurement device that can be moored or drifting. These devices can transfer acquired observations to the collection stations via satellite telecommunication systems for further analysis e.g., research work, forecasting weather, etc. [49]

Buoys without anchors are called drifting buoys. In general, drifting buoys are composed of a buoy and a drogue that are attached to a long and thin tether (Figure 2.1). The buoy floats on the ocean's surface and holds electronic devices such as batteries and sensors inside. The drogue, on the other hand, is an anchor under the water that has a multi-section cylinder full of holes. These holes, by creating small turbulences, improve the drifter's stability and slow down its slipstream speed [50]. Surface drifters, subsurface floats, and ice buoys are three different types of drifting buoys, all of which are independent of any type of anchor.

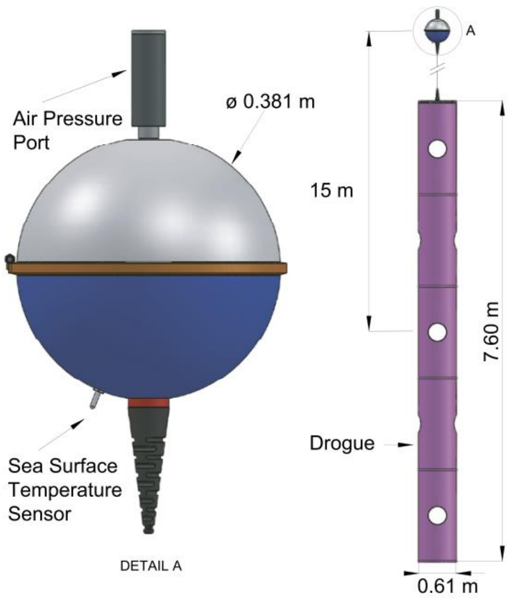

Figure 2. 1. A Drifting Buoy and its Drogue [49].

To observe surface current dynamics, surface drifters are utilized. These drifters can also provide information on salinity, speed and direction of surface winds, and air pressure. If they can be free of their drogue, they can be employed as a measurement tool for waves. Acoustic Doppler current profilers (ADCP) can also be attached to a surface drifter in the downward-looking state to record the drifter's motion [51].

Unmoored autonomous devices, which are used to measure currents, salinity, waves, and temperature of deep oceans, are called subsurface floats. By changing their buoyancy, they can change the depth of water they fluctuate in. This type of drifting buoy can carry an inertial motion unit to capture accelerations and tilts accurately. To send the recorded data, subsurface floats periodically rise to the surface of the ocean and send them, making use of their satellite antenna [2].

The last type of drifting buoy is ice buoys. They are mostly employed in the Arctic and Antarctic Seas to track their dynamic and thermodynamic evolution. Moreover, they can provide information on the variation of snow depth and ice thickness, the thermohaline structure of the ocean, and ice motion [52].

So much for drifting buoys. The other type of buoy to be reviewed is moored buoys. As it is obvious from the name of these buoys, they are anchored in fixed positions throughout the ocean. Therefore, the main application is for long-term observation, which includes various oceanographic measurement devices (Figure 2.2). Typical components of a moored buoy are the platform, electronic devices, sensors, power system, and mooring. Generally, there are two types of moored buoys: Translational buoys and pitch and roll buoys [2].

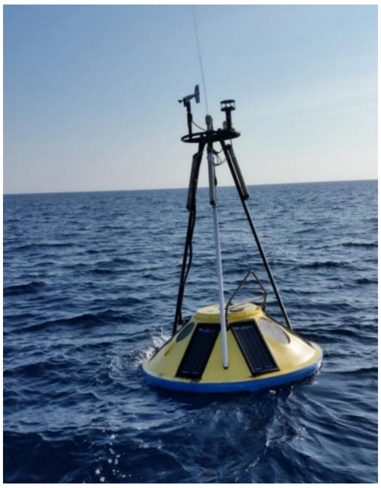

Figure 2. 2. A Moored Buoy [2].

Translational buoys, which are also called wave-following buoys due to their ability to follow the water particles, have a spherical shape in most cases. On the other hand, pitch and roll buoys, which are also called surface-following buoys due to their ability to follow the slopes, have a disc shape in most designs. To determine heave, pitch, and roll angles, a set of inertial sensors (tilt sensors and accelerometers) are used in these devices. These sensors can detect the buoy's axial acceleration, which by integrating it twice would result in the buoy's real-time position [2].

2.1.2 Satellite Observations

In order to observe inaccessible regions for in-situ measurements, satellite microwave remote sensing devices can be considered a special tool. To estimate ocean waves' height, they utilize the radar altimeter, which scatters pulses to the ocean's surface and measures the distance between the ocean's surface and the satellite [2].

Based on the presence or absence of an illumination source on the satellite, microwave satellite sensors can be classified into two categories: Passive and active sensors. In the former, naturally emitted electromagnetic data by the marine scene is captured by the sensor, meaning that the satellite does not have an illumination source. In the latter, the sensor's antenna emits an electromagnetic pulse and measures the reflected signal from the marine scene. These sensors can be used on both large-scale and small-scales. However, it should be mentioned that the scale indicates the spatial resolution of the results [2, 53].

2.1.3 Coastal Radars

Coastal radars are a type of remote sensor, which are placed on the land and can provide synoptic data with a high resolution. These sensors work based on the backscattered electromagnetic pulses from the surface of the ocean, in which they travel close to the surface of the ocean and the backscattered pulses are recorded. The backscattered electromagnetic pulses have a wavelength that is half that of the emitted pulses. The backscattered pulses are modified to obtain Doppler frequency and spectrum, which include first and second order echoes that can be further used to calculate the velocity of the surface currents and wave spectrum (Figure 2.3) [2]. Based on a relationship developed by [54, 55], the oceanic wave's main characteristics, such as its height, period, and mean direction, can be extracted from the backscattered pulses. They can be roughly divided into two types: Direction-finding and beam-forming systems. The former has a compact structure with closely spaced transceiving antennas, whereas the latter takes advantage of arrays of antennas. One can get more information on these sensors at [2].

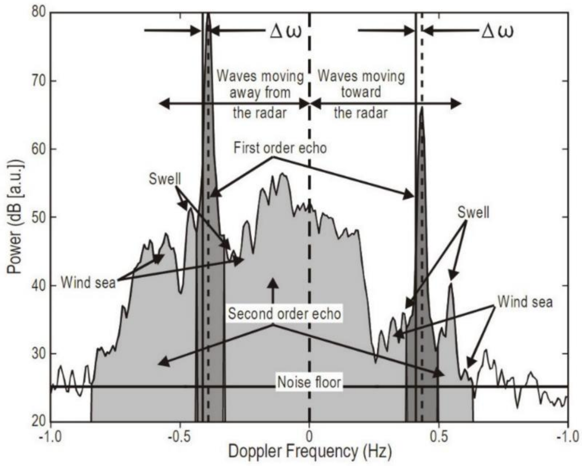

Figure 2. 3. Characteristics of a Remote Sensing Coastal Radar Signal [2]

2.1.4 Micro-Seism Analysis

Studying the micro-seism signals, which were considered noise in the past, can provide valuable information for human life. Mostly, the interaction between the ocean and solid Earth is the main reason for the generation of seismic signals on Earth. Based on the source of these signals, they can be classified into two main categories: Primary micro-seism and secondary micro-seism. Propagation of the oceanic waves over the slopes of the ocean base generates seismic waves that are called primary micro-seism. On the other hand, the non-linear interaction of the oceanic waves, which are traveling in opposite directions, would result in secondary micro-seism [56].

Several works can be found in the literature that have investigated the feasibility of using micro-seism signals for obtaining oceanic wave height. These measurements are mainly based on physics-based approaches, in which the micro-seism signals are linked to oceanic waves' height [57, 58].

2.1.5 Limitations of the Current Techniques

Each of the aforementioned techniques has its limitations. Buoys contain sensitive devices that can be easily damaged, e.g., the gyroscopes used in accelerometers are less reliable in the case of long-term operations. Also, having a long anchor in moored buoys causes problems for fishing in the oceans. Moreover, as the tensions can affect the movement of the buoys and should be avoided, they require careful mooring [2].

Although satellite microwave sensors can provide measurements on a large scale, they show imperfect radiometric, spatial, and spectral resolutions [2].

In the case of coastal radars, they show a low signal-to-noise ratio, which limits the accuracy of detecting lower wave heights. Moreover, they show limitations in defining the wave spectrum where there are very intense surface currents [59].

Micro-seism analysis could have difficulty in deriving the oceanic waves' information as they do not directly measure the ocean's state. Moreover, there would be difficulty in determining the exact location of the micro-seism sources, thus capturing the waves' information in an exact location can be cumbersome [2, 60].

2.2 Oceanic Piezoelectric Energy Harvesters

The two well-known piezoelectric effects, namely direct and converse piezoelectric effects, have led piezoelectricity to many different applications in both research and industry as actuators, sensors, and energy harvesters. Recently, piezoelectric materials have received remarkable attention in marine applications for energy harvesting from the ocean, which is a harsh environment with powerful and impactful waves and currents. However, to the best of the author's knowledge, although there are ample designs of piezoelectric energy harvesters in marine applications, piezoelectric material has not been employed for direct sensory and measurement applications in marine. Therefore, the literature on piezoelectricity in oceanic applications is limited to oceanic piezoelectric energy harvesters. An atlas-an innovative set of unified schematics and literature information-of 85 designs of piezoelectric energy harvesters in oceanic applications that have recently been reported in the state-of-the-art is provided. The following comprehensive atlas contains information on the utilized piezoelectric materials, piezoelectric coupling modes, location, power range, energy source, and a schematic of the piezoelectric energy harvesters design in oceanic engineering. It should be noted that all the information is collected exactly from the related references without any judgments and changes. The atlas includes just the information that the research articles provided, and in cases where there is no information in any of the atlas's sections, the related unit is free of information. Moreover, the atlas only includes designs for which they have at least provided a simulation or fabricated and tested a prototype. The schematics are sketched in a way to help future designers simply understand the working principles of the state-of-the-art. Table 2.1 shows the meaning of different colors in the schematics to fully understand the concepts. Tables 2.2, 2.3, 2.4, and 2.5 show the atlases of cantilever beam-based, diaphragm-based, stacked-based, and cymbal-based designs, respectively.

Table 2. 1. Meaning of Each Color in the Atlas.

Color	Meaning
	Buoy
	Magnet
	Piezoelectric Layer
	Water
The Other Colors	Non-Piezoelectric Material

Table 2. 2. Atlas of Cantilever Beam-Based Piezoelectric Energy Harvesters.

Year and Reference	Material	Coupling Mode	Location	Power Density (W/m^3)	Energy Source	Schematics
1987 [61]	PVDF	3-1	Onshore	-	Wave Motion	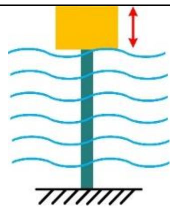
1987 [62]	PVDF	3-3	-	-	Wave Motion	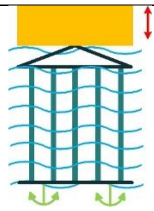
2001 [63]	PVDF	3-1	-	-	Water Current	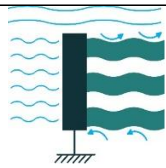
2004 [64]	PVDF	3-1	-	-	Water Current	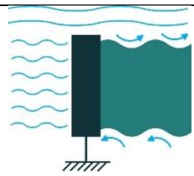
2004 [64]	PZT	3-1	-	7 × 10	Water Current	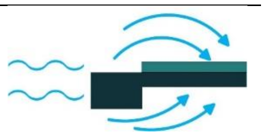

2007 [65]	PVDF	3-1	Onshore	-	Water Current	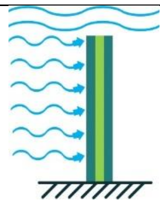
2009 [66]	-	-	Offshore	1.646	Wave Motion	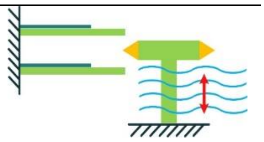
2010 [67]	PVDF	3-3	Offshore	1.5×10	Water Current	
2011 [68]	PVDF	-	Offshore	4×10^{-3}	Water Current	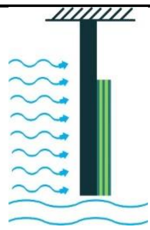
2012 [69] [70]	PVDF	-	Offshore	4.2×10^{-1}	Wave Motion-Water Current	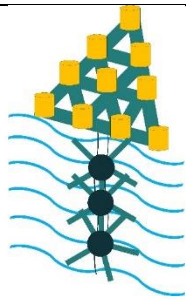
2012 [71]	-	-	-	1.56×10^{-4}	Water Current	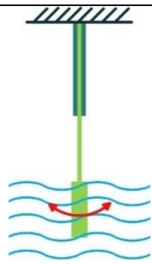
2012 [72]	PZT	3-1	Onshore	1.721×10^{-1}	Wave Motion	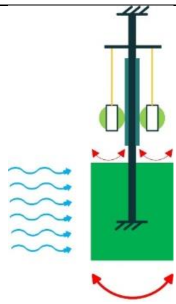

2013 [73]	PZT	3-3	-	8.395×10^{-1}	Water Current	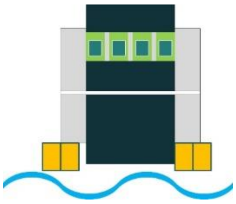
2013 [74]	PZT	-	-	3.66×10^{2}	Wave Motion	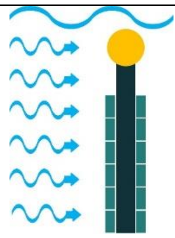
2014 [75]	PZT	-	Offshore	7.5×10	Wave Motion	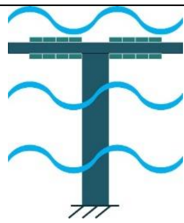
2014 [76]	PZT	3-3	-	4.74	Wave Motion	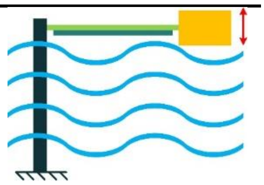
2014 [77]	PVDF	3-1	-	-	Water Current	
2015 [78]	MFC	3-1	-	1.16×10^{-2}	Water Current	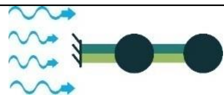
2015 [79]	PZT	3-1	-	2.24×10^{-2}	Water Current	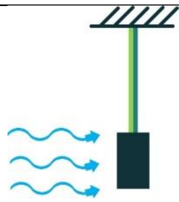
2015 [80]	PZT	-	-	-	Water Current	
2015 [81]	PVDF	-	-	-	Water Current	
2015 [82]	PVDF	3-1	-	1.65×10^{-4}	Water Current	

2015 [83]	PZT	-	Near/Offshore	1.276	Wave Motion	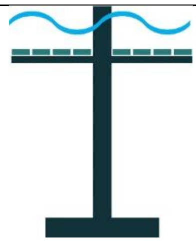
2015 [84]	-	-	Nearshore	3.5×10^{-10}	Wave Motion	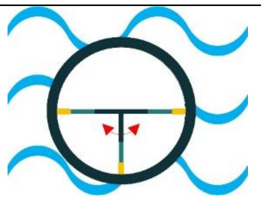
2015 [85]	MFC	-	-	6.1×10^{-3}	Water Current	
2016 [86]	PZT	3-1	-	1.731×10	Water Current	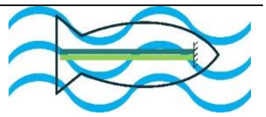
2016 [87]	PZT	3-3	Near/Offshore	2.06×10^{2}	Wave Motion	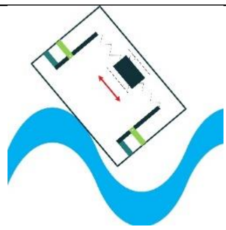
2016 [88]	PVDF	-	-	5.797×10^{-1}	Water Current	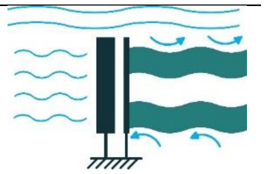
2016 [88]	PZT	-	-	5.797×10^{-1}	Water Current	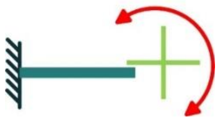
2016 [89]	PVDF	3-1	Near/Offshore	-	Wave Motion	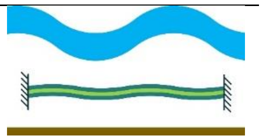
2017 [90]	PVDF	3-1	Near/Offshore	2.6×10^{-12}	Water Current	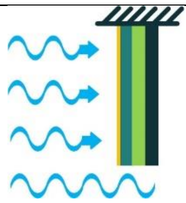

2017 [91]	PZT	-	-	1.4	Water Current	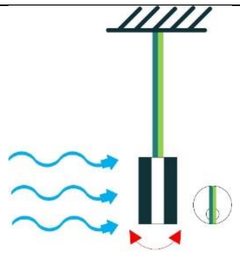
2017 [92]	PZT	-	-	1.598×10^4	Wave Motion	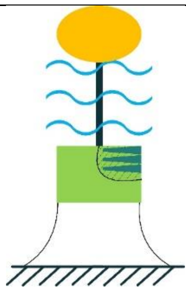
2017 [93]	PZT	-	-	1.4354×10^2	Wave Motion	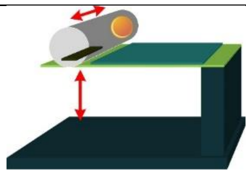
2017 [94]	PZT	3-3	On/Near/Off shore	2.6×10^2	Wave Motion	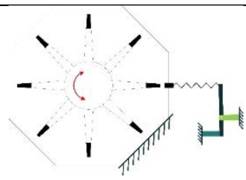
2017 [95] [96]	PZT	3-1	-	3.5×10^{-8}	Water Current	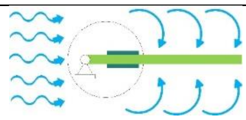
2018 [97]	PZT	3-1	-	-	Wave Motion	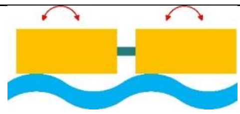
2018 [98]	PZT	-	Offshore	1.034×10^4	Wave Motion	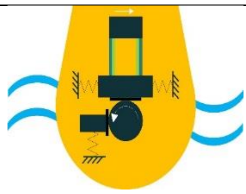
2018 [99]	-	3-3	-	2.4×10^3	Wave Motion	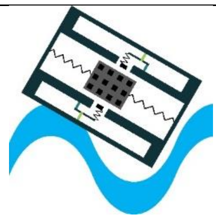
2018 [100]	MFC	3-1	-	-	Water Current	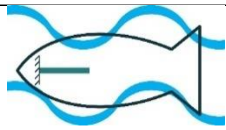

2018 [101]	-	-	-	2.56	Water Current	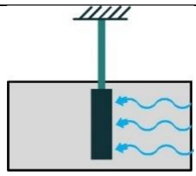
2019 [102]	-	-	-	-	Wave Motion	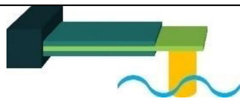
2019 [103]	PZT	3-3 & 1-5	-	1.447×10^{-1}	Water Current	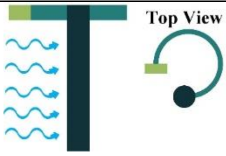
2019 [104]	PZT	3-3	Offshore	4.77×10^{2}	Wave Motion	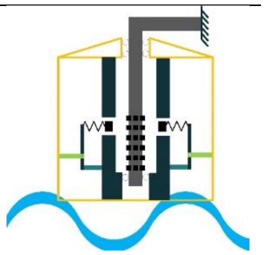
2019 [105]	PZT	3-1	-	-	-	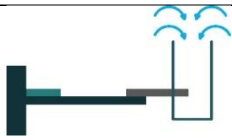
2019 [106]	PZT	-	Nearshore	1.06×10^{4}	Wave Motion	
2019 [21]	-	3-1	Onshore	-	Wave Impact	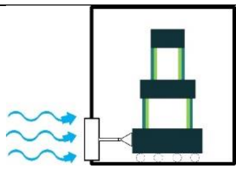
2019 [107]	PVDF	3-1	Offshore	2×10^{-7}	Wave Motion	
2019 [108]	-	-	-	-	Water Current	

2019 [109]	MFC	-	-	7.582×10^{-9}	Water Current	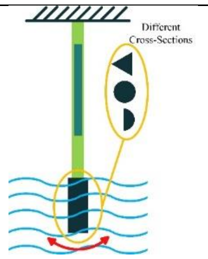
2019 [110]	MFC	-	-	-	Water Current	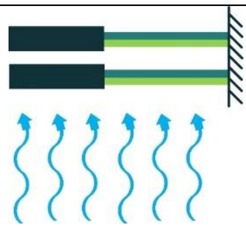
2019 [111]	PZT	-	-	-	Water Current	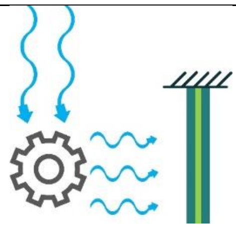
2019 [112]	PZT	-	Offshore	1.4×10^{2}	Wave Motion	
2020 [113]	PVDF	-	-	-	Water Current	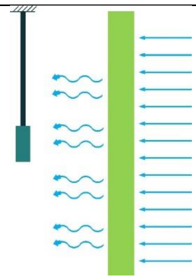
2020 [114]	PZT	3-1	-	7.346×10^{-2}	Water Current	
2020 [115]	MFC	-	-	-	Water Current	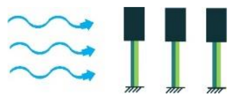
2020 [116]	PZT	-	-	-	Wave Motion	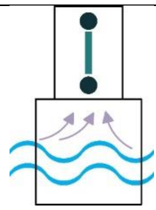
2020 [117]	PVDF	-	-	-	Water Current	

2020 [118]	PZT	-	-	5.74×10^{-8}	Water Current	
2021 [119]	-	-	-	1.29×10^{1}	Wave Motion	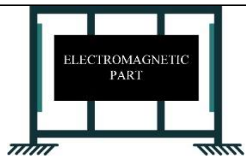
2021 [120]	PZT	-	-	8.425×10^{-4}	Water Current	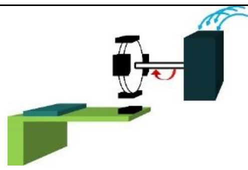
2021 [121]	PZT/PVDF	-	Near/Offshore	1.050×10^{3}	Wave Motion	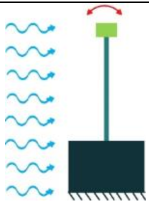
2021 [122]	MFC	3-1	-	1.074×10^{3}	Water Current	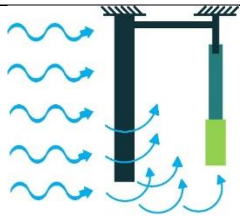
2021 [123]	PVDF	3-1	-	-	Wave Motion	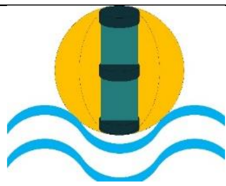
2021 [124]	PZT	-	-	3.587×10^{-2}	Water Current	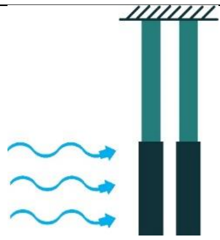
2021 [125]	-	-	-	3.2×10^{-3}	Wave Motion	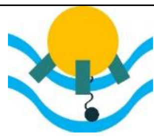
2021 [126]	PZT	-	-	1.632	Wave Motion	
2021 [127]	-	-	-	-	Wave Motion	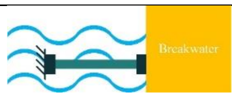
2021 [128]	PZT/MFC	-	-	62×10^{3}	Wave Motion	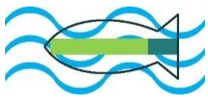

2021 [129]	PZT	-	Offshore	-	Wave Motion	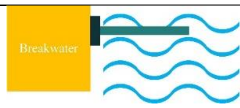
2021 [130]	PZT	-	-	-	Wave Motion	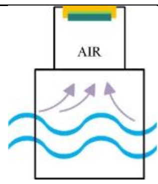
2021 [131]	-	-	Nearshore	-	Wave Motion	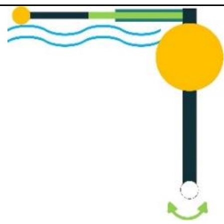
2021 [132]	MFC	3-3	-	8.5×10^{-3}	Wave Motion	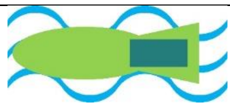

Table 2. 3. Atlas of Diaphragm-Based Piezoelectric Energy Harvesters.

Year and Reference	Material	Coupling Mode	Location	Power Density (W/m³)	Energy Source	Schematics
2010 [133]	PVDF	3-1	-	1.9×10^{-2}	Water Current	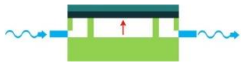
2011 [134]	PZT	1-5	-	7.258×10^{-5}	Water Current	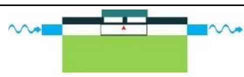
2013 [135]	PZT	-	Offshore	3.453×10^{-1}	Water Current	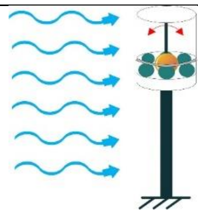
2013 [136]	PZT	-	Offshore	-	Wave Motion	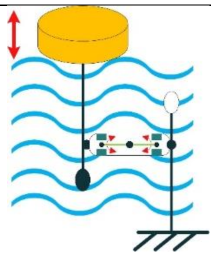
2013 [137]	PZT	-	Offshore	-	Wave Motion	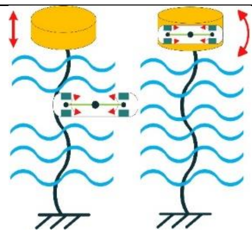

2018 [138]	PZT	3-3	-	-	Water Current	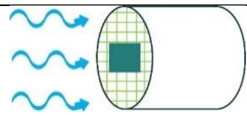
2019 [139]	PVDF	-	-	5.681×10^{-2}	Wave Motion	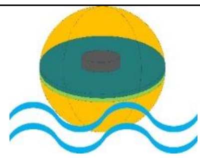

Table 2. 4. Atlas of Stacked-Based Piezoelectric Energy Harvesters.

Year and Reference	Material	Coupling Mode	Location	Power Density (W/m³)	Energy Source	Schematics
2013 [39]	PVDF	3-3	-	-	Wave Impact	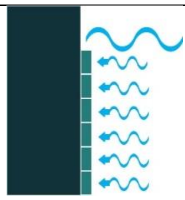
2017 [140]	PZT	-	Offshore	6×10^{2}	Wave Impact	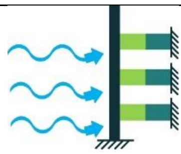
2021 [141]	PZT	-	-	-	Wave Motion	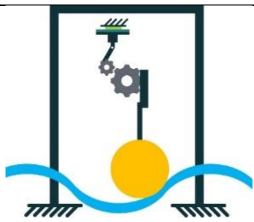

Table 2. 5. Atlas of Cymbal-Based Piezoelectric Energy Harvesters.

Year and Reference	Material	Coupling Mode	Location	Power Density (W/m³)	Energy Source	Schematics
2010 [142]	PZT	3-3	-	2.526×10^{1}	Water Current	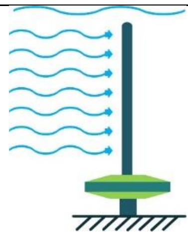
2021 [143]	PZT	-	-	2.038×10^{1}	Water Current	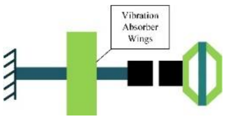

2.3 Summary

This Chapter is dedicated to providing information on the literature on piezoelectric sensors in oceanic applications. However, as there was not even a single work on the piezoelectric sensors in oceanic applications, the literature on the present ocean waves measurement devices has been reviewed, and their limitations extracted. Then, oceanic piezoelectric energy harvesters as the only application of piezoelectric materials in oceanic applications have been reviewed and a comprehensive Atlas is provided, which includes information on the utilized piezoelectric materials, piezoelectric coupling modes, location, power range, energy source, and a unified schematic of the piezoelectric energy harvesters design in oceanic applications. As reviewed in Tables 2.2 to 2.5, piezoelectric energy harvesters are generating very small power and, in most cases, it is in mW range, which can be used to power a low-power sensor or charge a battery. Taking advantage of them, a direct measurement-based sensor can be developed that is free of battery replacement or recharge.

3. Design of the Drifter-Based Self-Powered Piezoelectric Sensor

Many piezoelectric sensors have been designed over time, employing the direct piezoelectric effect. Here, taking advantage of a drifter, a piezoelectric sensor is designed to capture ocean waves' height and period. Moreover, the output electrical pulses will be used to power the sensor. This Chapter discusses the configuration of the proposed sensor as well as its working principle.

3.1 Configuration of the Proposed Sensor

In the present sensor, a drifter is employed to carry the sensor and help it float on the ocean surface. Ocean waves drive the drifter up and down by applying forces to it. Consequently, the drifter applies forces to the piezoelectric material to change its state of motion. Figure 3.1 (a) shows a schematic of the proposed drifter-based piezoelectric sensor. It consists of a drifter, a piezoelectric disk, a battery, a microprocessor, and a glass cover (Figure 3.1 (b)). As discussed in Chapter 1, piezoelectric materials generate electricity in response to mechanical stresses. Therefore, the output voltage can be used to capture ocean waves' height and period. Moreover, this electrical energy can be stored in a battery and further used to power the sensor and send the captured data to a nearby station (Figure 3.2). The glass cover is also used to seal the electronics against ocean water.

Figure 3.3 shows some indicative dimensioning of the proposed drifter-based piezoelectric sensor.

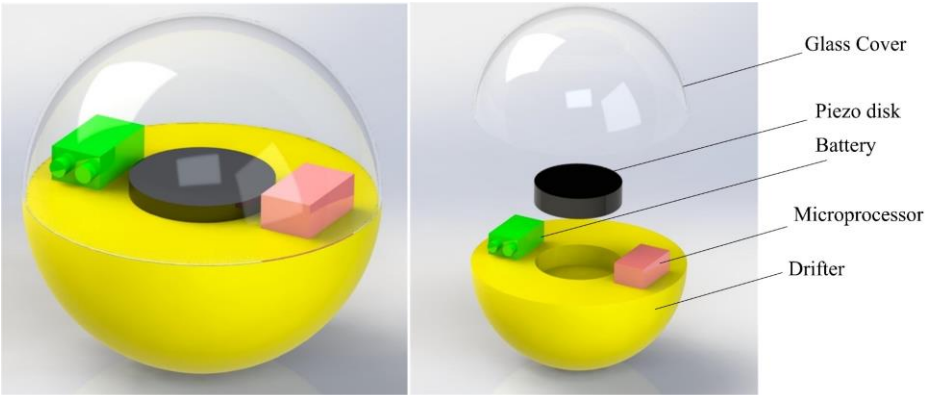

(a) **(b)**

Figure 3. 1. (a) Proposed Drifter-based Self-Powered Piezoelectric Sensor for Ocean Wave Measurement; (b) The Sensor's Components

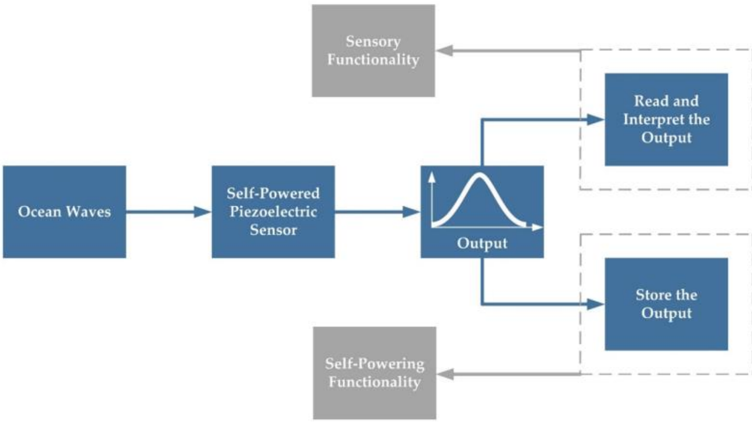

Figure 3. 2. Working Principle of the Drifter-Based Self-Powered Piezoelectric Sensor

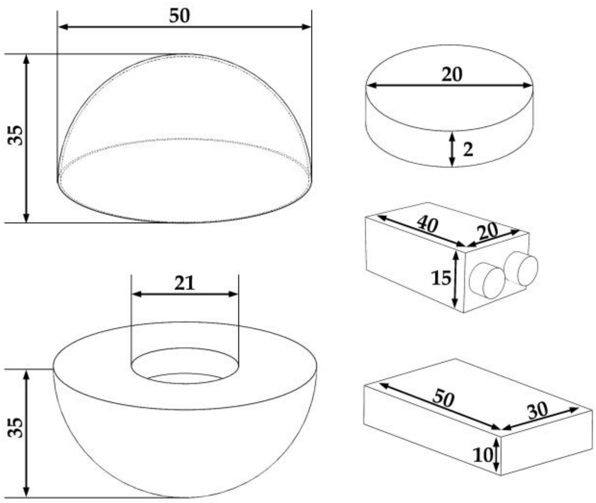

Figure 3. 3. Indicative Dimensioning of the Proposed Drifter-Based Self-Powered Piezoelectric Sensor

3.2 Working Principle

The proposed drifter-based piezoelectric sensor works based on Newton's laws of motion, in which an object resists any changes in its state of motion due to its mass. Ocean waves start to fluctuate and apply force to the drifter and, consequently, to the piezoelectric disk to change their state of motion. Because of inertia, they resist changing their state of motion, and thus the piezoelectric disk deforms due to this force and generates electricity in response to it. The generated electrical pulses can be used to power the sensor (charge the battery) and capture wave height and period. After powering the battery, the sensor can send the output data to a nearby station for further analysis.

The working steps of the proposed drifter-based piezoelectric sensor is as follows (Figure 3.4):

- **At the time t_0:** The ocean waves are at rest and the forces are in balance (Figure 3.4 (a));
- **From time t_0 to t_1:** Ocean waves go up and apply force to the drifter and the piezoelectric disk to change their state of motion. Resistance to this change would result in the deformation of the piezoelectric disk and electricity generation (Figure 3.4 (b));
- **From time t_1 to t_2:** After a while, ocean waves gradually subside, resulting in a reduction in the forces on the piezoelectric disk (Figure 3.4 (c));
- **At the time t_2:** The ocean waves are at rest again and the forces are in balance (Figure 3.4 (d));

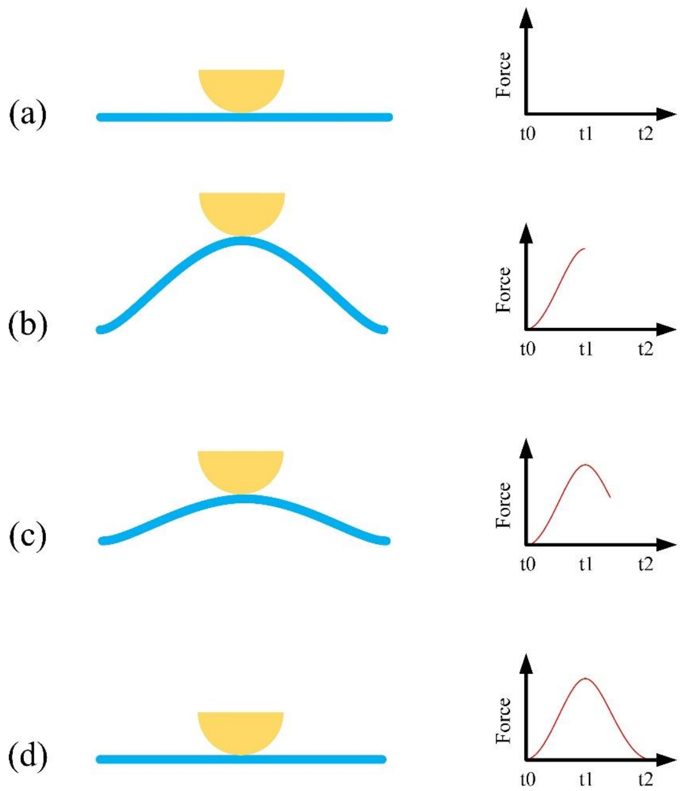

Figure 3. 4. Working Steps of the Drifter-based Piezoelectric Sensor.

3.3 Summary

This Chapter provided the detailed configuration of the proposed piezoelectric sensor and its working principle by illustrating them. It is also discussed that the proposed sensor works based on the law of inertia and changing the state of motion of the piezoelectric material. Considering this law, a step-by-step working principle is provided to describe the way it works.

4. Modeling and Analysis

This Chapter analyzes the motion principle and the working performance of the proposed drifter-based piezoelectric sensor using a dynamic model. Moreover, taking advantage of the commercial software COMSOL-Multiphysics, finite element analysis (FEA) has been carried out to verify the results of the proposed dynamic model.

4.1 Dynamic Modeling

The masses, the springs, and the dampers are the main parts of a mechanical system. For a mechanical system, these three elements are the basic actuators to understand the nature of the motion principle. Here, the well-known mass-spring-damper system is employed for analyzing the working performance of the proposed piezoelectric sensor, in which masses are distributed using a set of springs and dampers.

4.1.1 Construction of the Dynamic Model

Based on Newton's second law of motion, a dynamic model is established to analyze the motion principle and the working performance of the proposed drifter-based piezoelectric sensor. The main purpose of this modeling is to analyze the system's response (the output) to an input of ocean waves. In the first step, the contact force on the piezoelectric material is calculated, and then it is substituted into the related equations to obtain the output voltages. Figure 4.1 (a) shows the steps of the dynamic modelling from ocean waves to the output voltages.

Schematics of a dynamic model and its free-body diagram are illustrated in Figure 4.1 (b). A damped spring-mass system is utilized to investigate the dynamic performance of the proposed sensor. The mass, stiffness, displacement, and damping coefficient of the piezoelectric disk are represented by M_P, K_P, Y_P, and C_P, respectively. Moreover, the mass, stiffness, and displacement of the drifter are M_d, K_d, and Y_d, respectively. Y_w, also denotes the motion of the ocean waves.

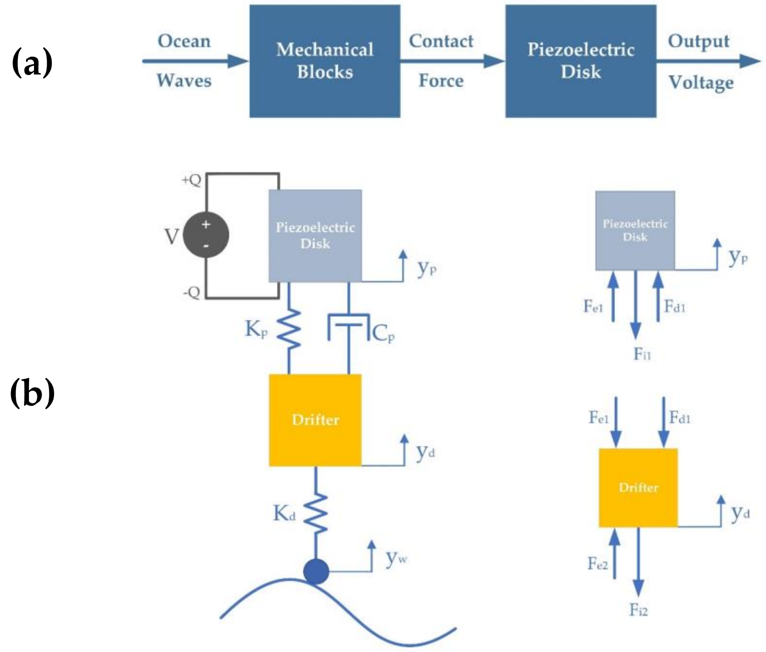

Figure 4. 1. (a) Steps of the Dynamic Modelling from Ocean Waves to the Output Voltages; (b) Schematics of the Proposed Dynamic Model and its Free-Body Diagram.

where in Figure 4.1:

F_{i1}= piezoelectric disk's inertial force;

F_{i2}= drifter's inertial force;

F_{e1}= piezoelectric disk's elastic force;

F_{e2}= drifter's elastic force;

F_{d1}= piezoelectric disk's damping force.

The direction of the forces is set by considering the following: The ocean waves have a motion like a sine wave, which causes the sensor to move in the same way. The force acting on the drifter from the waves will cause it to compress. This will generate an elastic force, F_{e2}, which will push the drifter up. Due to inertia, the drifter will try to resist the position change through the inertial force F_{i2}. The elastic force is also acting on the ocean waves, but this is not in the interest of this study. The piezoelectric disk will oppose the upward movement of the drifter and will push on it with the elastic force F_{e1} and the damping force F_{d1}. According to Newton's third law of motion, for each action, there is a reaction. Therefore, the elastic force F_{e1} and the damping force F_{d1} will push the piezoelectric disk upwards. Due to inertia, the body's mass will try to resist the position change through the inertial force F_{i1}.

The equation of force equilibrium for the piezoelectric disk is:

$$F_{i1} = F_{e1} + F_{d1}, \tag{4.1}$$

The inertial force, the elastic and damping forces of the piezoelectric disk are expressed as:

$$F_{i1} = M_p \ddot{y}_p, \tag{4.2}$$

$$F_{d1} = C_p(\dot{y}_c - \dot{y}_p), \tag{4.3}$$

$$F_{e1} = K_p(y_c - y_p), \tag{4.4}$$

Replacing the expressions of the forces in equation (4.1), we get:

$$M_p \ddot{y}_p = C_p(\dot{y}_d - \dot{y}_p) + K_p(y_d - y_p), \tag{4.5}$$

The equation of force equilibrium for the drifter is:

$$F_{i2} + F_{e1} + F_{d1} = F_{e2}, \tag{4.6}$$

The inertial force, the elastic and damping forces of the drifter are expressed as:

$$F_{i2} = M_d \ddot{y}_d, \tag{4.7}$$

$$F_{e2} = K_d(y_w - y_d), \tag{4.8}$$

Substituting the expressions of the forces in equation (4.6), we have:

$$M_d \ddot{y}_d + C_p(\dot{y}_d - \dot{y}_p) + K_p(y_d - y_p) = K_d(y_w - y_d) \quad , \tag{4.9}$$

Applying the contact force ($F_{e1} = K_p(y_c - y_p)$ and $F_{d1} = C_p(\dot{y}_c - \dot{y}_p)$) on the piezoelectric disk by substituting it in the following equations (Equations (4.10) to (4.12)) [144] will give us the output voltage generated:

$$V = \frac{Q}{C}, \tag{4.10}$$

where V, Q, and C are voltage, charge, and capacitance of the piezoelectric disk, respectively. Q and C can be simplified even more to the following equations [145]:

$$Q = d_{33} \times F, \tag{4.11}$$

$$C = \frac{\varepsilon_r \varepsilon_0 A}{t}, \tag{4.12}$$

where d_{33}, F, ε_r, ε_0, A, and t represent piezoelectric coefficient, contact force, relative permittivity, vacuum permittivity, area, and thickness, respectively.

Moreover, from the following equations, mass and stiffness for both the drifter and piezoelectric disk can be calculated, and the damping and piezoelectric coefficients of the piezoelectric disk can be taken from the references:

$$\rho = \frac{M}{v}, \tag{4.13}$$

$$K = E\frac{A}{l}, \tag{4.14}$$

where ρ and v are the density and volume of the material, and E, A, and l stand for Young's modulus, area, and length of the material, respectively.

4.1.2 Results

Taking advantage of the MATLAB/Simulink modulus, the aforementioned proposed dynamic model is simulated. Table 1 shows the parameters used in the simulation. Some of them are taken from the literature, and some others are based on the prototype and FEA model. It should also be noted that the damping and stiffness of the piezoelectric disk are assumed to be linear and the uni-axial stiffness of the disk, respectively. Further, Polyvinyl Chloride (PVC) material is employed for the drifter in the simulations.

Table 4. 1. Parameters Used in the MATLAB/Simulink Simulation

Parameter	Value	Parameter	Value
d_{33}	2.89×10^{-10} m/V	The Density of Piezo	7500 kg/m^3
ε_r	1300	The Density of the Drifter	1760 kg/m^3
ε_0	8.85×10^{-12}	Diameter of the Drifter	40.00×10^{-3} m
Thickness of Piezo	1.00×10^{-3} m	Height of the Drifter	10.00×10^{-3} m
Area of Piezo	3.14×10^{-4} m^2		

Figure 4.2 shows the input waves to the developed dynamic model (Figure 4.2 (a)) and the resulting output voltages (Figure 4.2 (b)). for ocean waves with a 0.2 to 0.5 m height and a 3.5 s period. The wave parameters, height and period, are mostly dependent on the seasonality and geographic location. However, for simplicity, heights of 0.2 to 0.5 m with a period of 3.5 s have been chosen for the analysis as these parameters are frequent in all locations and seasons.

(a)

(b)

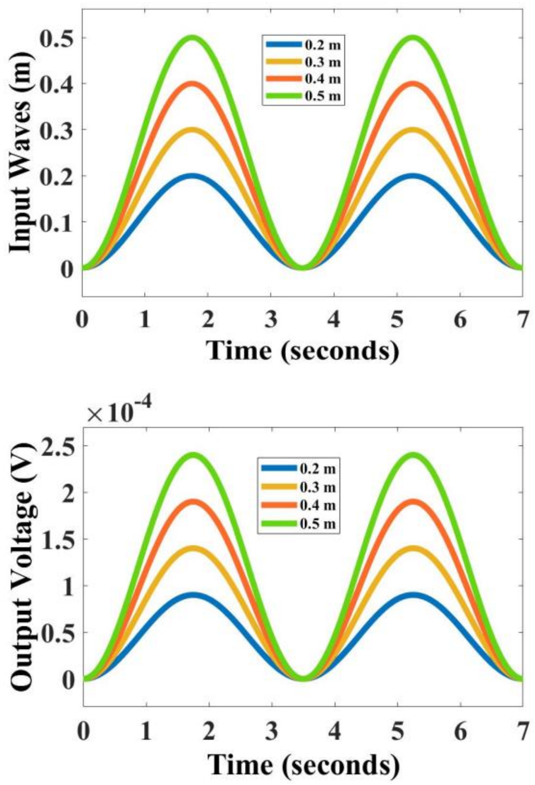

Figure 4. 2. Input Waves and Output Voltages: (a) Input Ocean waves of 0.2 to 0.5 m in Height; (b) Output Voltages for Ocean Waves of 0.2 m (Blue Line), 0.3 m (Orange Line), 0.4 m (Red Line), and 0.5 m (Green Line) Height

The peak values of output voltages are 90 μV, 140 μV, 190 μV, and 240 μV for input waves with 0.2 m, 0.3 m, 0.4 m, and 0.5 m height, respectively. A 3.5 s period is chosen for all input waves to the dynamic model.

As mentioned, two main characteristics of each wave are its height and period to be measured. Results shown in Figure 4.2, show that the height of the input waves has a linear relationship with the output voltage's amplitude. However, the period of the inputs was all set to a constant value. Therefore, it is required to compare input waves and output sinusoidal voltages' periods to each other. To do so, the input waves' height is set to a constant value and the periods are considered variables. A height of 0.5 m with periods of 1.5 s, 2.5 s, 3.5 s, 4.5 s, and 5.5 s were chosen for this analysis. The results are shown in Figure 4.3.

As it is clear in Figure 4.3, the period of the input waves is the same as the output voltages, meaning that the amplitude of the output voltage is the only factor that needs to be interpreted to obtain a wave's characteristics.

(a)

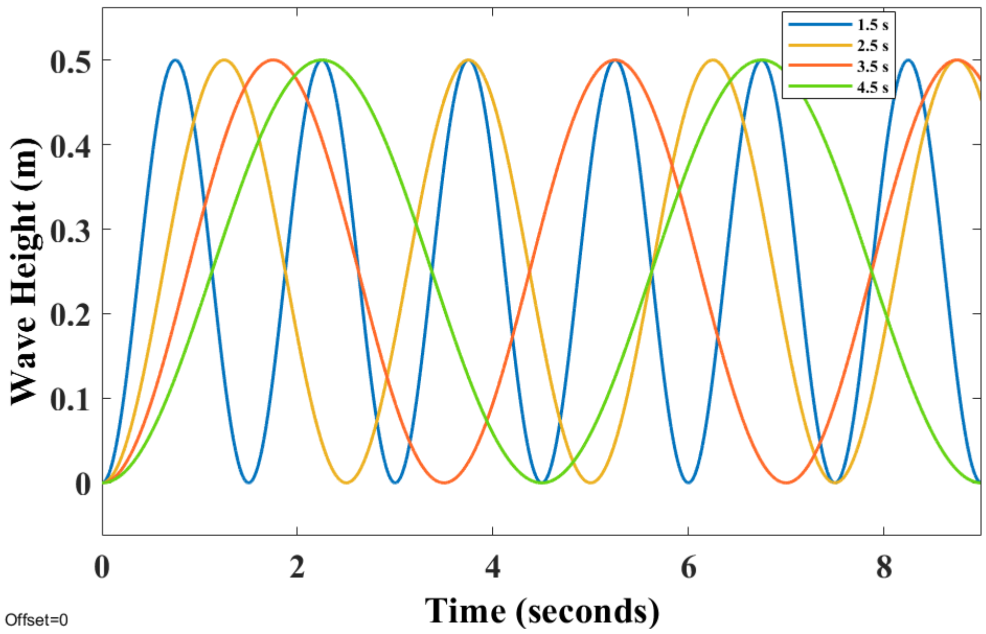

(b)

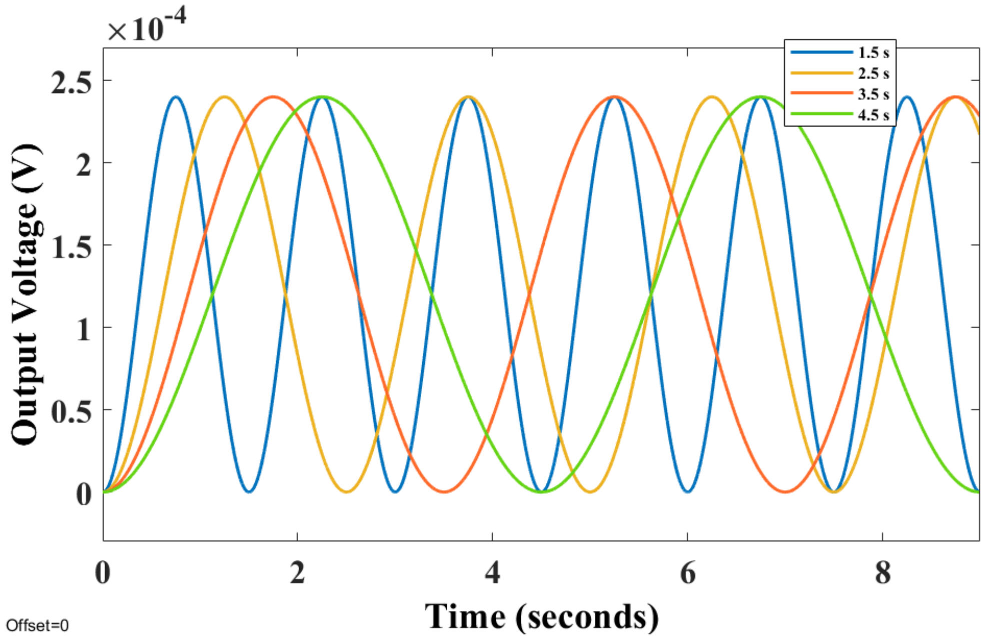

Figure 4. 3. Impact of the Period on the Output Voltage: (a) Input Waves; (b) Output Voltages.

4.2 Finite Element Analysis (FEA)

As a computerized method, finite element analysis (FEA) predicts a design's reaction to different types of forces. Here, the model contains both mechanical and electrostatic forces as inputs and outputs, respectively. Therefore, a coupled-physics analysis should be carried out to investigate the output voltages for the input ocean waves. To do so, COMSOL-Multiphysics has been employed to carry out the FEA simulations to verify the proposed dynamic model.

4.2.1 Construction of the Coupled-Physics FEA Model

Making use of the commercial software COMSOL-Multiphysics, an FEA simulation has been carried out to further verify the feasibility of the designed drifter-based piezoelectric sensor.

The proposed sensor works under the applied mechanical load coming from the ocean waves and converts the inputs to electrical pulses using piezoelectric material. Therefore, a coupled physics analysis of "Solid Mechanics" and "Electrostatics" Modules should be employed to simulate the piezoelectric sensor and achieve the output voltages.

The selected materials in this simulation are Lead Zirconate Titanate (PZT-4) and Polyvinyl Chloride (PVC) for piezoelectric material and the drifter, respectively. For meshing the structure, a "Finer" element size is selected. To define piezoelectric electrodes, a Ground node is applied on the lower side of the piezoelectric material, and a Floating Potential node is applied on its upper side. A Contact Pair is utilized to define the contact between the piezoelectric disk and the drifter. Then, volume forces (gravity) are applied to both of them to prevent any sudden jump when subjected to the force of the ocean waves. Finally, a prescribed motion with a sinusoidal function is applied to the drifter to mimic the ocean waves, which is the input of the system. Details of the steps of the FEA model can be found in Figure 4.4. Moreover, Figure 4.5 shows a screenshot of the whole model builder and the meshed model.

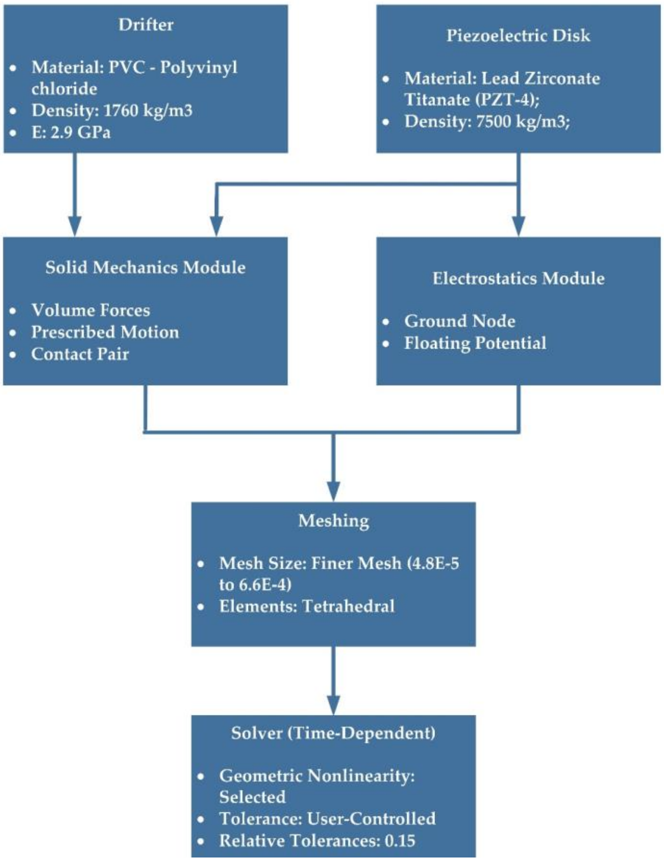

Figure 4. 4. The Flowchart of the FEA Simulation in COMSOL.

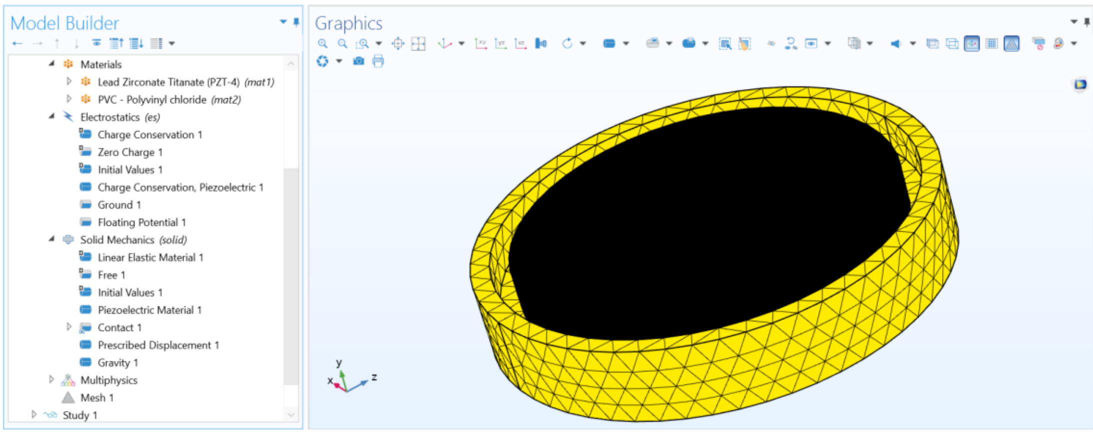

Figure 4. 5. Screenshot of COMSOL-Multiphysics Model

4.2.2 Simulation Results

Based on the mentioned inputs, the simulations are carried out. The sensor, meshed model, and results of simulations are shown in Figure 4.6.

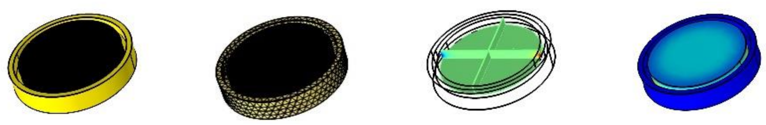

(a)

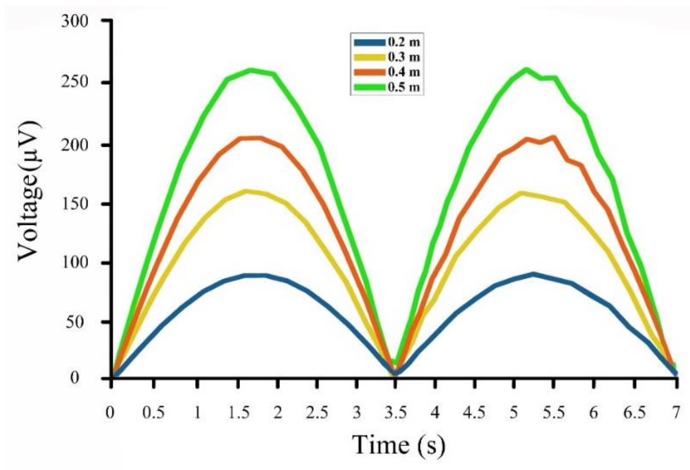

(b)

Figure 4. 6. COMSOL Models and Results: (a) The Model, Meshed Model, Electrical Potential Output, and Stress Output; (b) Output Voltages for Ocean Waves of 0.2 m (Blue Line), 0.3 m (Yellow Line), 0.4 m (Red Line), 0.5 m (Green Line) Height.

As can be seen in Figure 4.6, the results of the FEA simulations for the proposed drifter-based piezoelectric sensor in the commercial software COMSOL Multiphysics are a bit higher than the proposed dynamic model. The peak values for the output voltage are 95 μV, 160 μV, 205 μV, and 260 μV for input ocean waves of 0.2 m, 0.3 m, 0.4 m, and 0.5 m in height, respectively. It should also be noted that the period of the input wave for all of the above-mentioned simulations is 3.5 s, and as it is clear in Figure 4.5, the periods are the same for both inputs and outputs.

4.3 Summary

To investigate the proposed piezoelectric sensor's feasibility, a dynamic model based on a mass-spring-damper system is proposed in this Chapter and is verified by a coupled-physics analysis in COMSOL-Multiphysics. For an input wave of 0.2 m, 0.3 m, 0.4 m, and 0.5 m in height and 3.5 s in period, the calculated output voltages using the dynamic model are 90 μV, 140 μV, 190 μV, and 240 μV, respectively, whereas the output voltages of the FEA simulations are 95 μV, 160 μV, 205 μV, and 260 μV for the same input waves.

Furthermore, periods of input waves and output sinusoidal voltages are compared using the dynamic model. The period of the input waves is the same as the output voltages, meaning that the amplitude of the output voltage is the only factor that needs to be interpreted to obtain a wave's characteristics.

5. Prototype Fabrication and Testing

This Chapter is dedicated to the prototype fabrication and testing of it to verify the results of the developed dynamic and FEA models. This experiment is composed of two parts: 1) Mimicking ocean waves and 2) Testing the sensor. In the former, a slider-crank mechanism is utilized to represent ocean waves, whereas in the latter, the performance of the proposed piezoelectric sensor is investigated.

5.1 Slider-Crank Mechanism

As discussed in Section 1.5 and illustrated in Figure 1.3, height and period are the two main characteristics of an oceanic wave. Here, efforts are made to mimic these two characteristics for testing the proposed piezoelectric sensor. To simulate the motion of the ocean waves, a slider-crank mechanism is employed, in which the circular velocity of a motor represents the ocean waves' period, and its diameter stands for the waves' height (Figure 5.1). Simply speaking, the diameter of the disk specifies how much the distance between a wave's crest and trough is, and its rotational velocity determines the wave's period (frequency). Therefore, tuning the circular velocity of the motor would result in different ocean wave periods, and changing the diameter of the disk in the mechanism can change the wave's height.

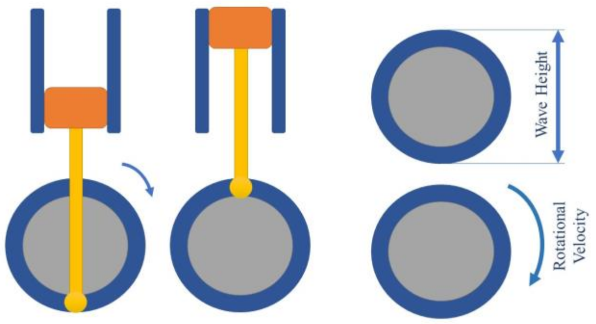

Figure 5. 1. Slider-Crank Mechanism to Mimic Ocean Waves

5.2 Prototype of the Proposed Sensor

As shown in Figure 5.2 (a), the experimental setup includes a slider-crank mechanism, a servo motor, the proposed sensor, an Arduino board, and a Personal Computer (PC) as the data acquisition device. The fabricated sensor is shown in Figure 5.2 (b), in which a piezoelectric disk (a buzzer element STD 35mm manufactured by Murata Electronics) is nested inside a plastic container that represents the drifter shown in Figure 3.1. The programs for the servo motor's motion are programmed on the PC and then uploaded to the Arduino board. Taking orders from the board, the servo motor starts working with the determined rotational velocity. Then, the slider-crank mechanism represents the ocean waves and pushes the piezoelectric sensor up. The output voltage of the piezoelectric sensor is recorded by the Arduino board and sent back to the PC.

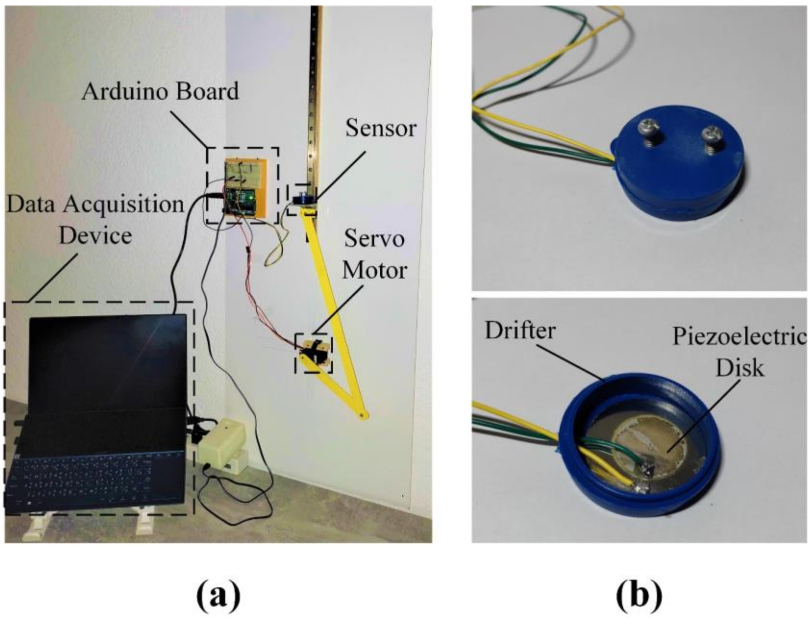

Figure 5. 2. (a) Experimental Setup; (b) The Fabricated Sensor Prototype for Testing.

5.3 Experimental Results

Two waves are simulated using the slider-crank mechanism: 1) A wave with a height of 0.2 m and a period of 3.5 seconds; and 2) A wave with a height of 0.3 m and a period of 3.5 seconds. It should be mentioned that the experiment is limited to these two waves due to the employed servo motor's limitation in providing higher loads and the experimental setup. The results of the tests for the two waves are shown in Figure 5.3, in which the blue line and orange line represent the experimental results for waves with a height of 0.2 m and 0.3 m, respectively, both with a period of 3.5 seconds. This Figure shows the results of the simulation for the ocean waves with a period of 3.5 s and heights of 0.2 m and 0.3 m. The peak voltage values are 92 μV and 155 μV for waves with a height of 0.2 m and 0.3 m, respectively.

The output results of the experimental setup are mainly affected by the coarse and non-linear motion of the slider-crank mechanism. As it is clear from Figure 5.3, the slider-crank mechanism can carry the sensor up with a bit of noise. Moreover, due to the action of gravity, it comes down very fast. Fortunately, the proposed sensor could also successfully plot these results as well.

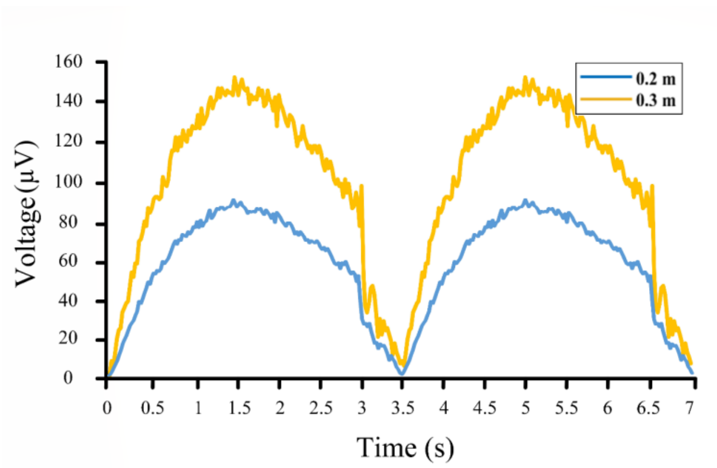

Figure 5. 3. Results of the Fabricated Prototype for Waves of 0.2 m (Blue Line) and 0.3 m (Orange Line) Height with a 3.5 s Period.

5.4 Summary

In this Chapter, the method of mimicking the ocean waves using a slider-crank mechanism is explained. Then, the experimental setup is shown and discussed. Finally, the results of the experiments are plotted, in which peak voltage values of 92 μV and 155 μV for waves with a height of 0.2 m and 0.3 m, respectively, have been obtained.

6. Results and Discussions

Chapters 4 and 5 have resulted in the output voltages for different ocean waves. This Chapter discusses several factors based on the extracted outputs:

1) Although the output voltages are shown in the previous Chapters, the relationship between the output voltages and the ocean waves is not explained. Therefore, in a Section in this Chapter, the output voltages are interpreted;
2) There are three output results (dynamic modeling, FEA simulation, and the experiment) for the proposed piezoelectric sensor. The results are compared in a Section to extract errors and confirm the feasibility of the piezoelectric sensor;
3) In another Section, the resolution of the sensor is investigated to see the smallest wave that it can measure;
4) Finally, the self-powering functionality of the sensor is discussed.

6.1 Interpretation of the Outputs

To estimate a wave's energy, its height and period should be measured precisely. Here, the proposed drifter-based piezoelectric sensor can respond to any small changes in these two elements. However, the recorded output data is electrical pulses (voltage) and should be further simplified and interpreted to show the ocean wave's characteristics (height and period). As it is clear from the dynamic model, FEA simulation, and experimental results (Figures 4.2, 4.4, and 5.3), the wave's period is the same as the output voltage of the piezoelectric material. On the other hand, based on the results of the dynamic model, there is a linear relationship between the output voltage and the wave height for different input waves (Figure 6.1). Therefore, the wave height can also be calculated simply from the output voltage of the proposed piezoelectric sensor. For example, considering the results of the proposed dynamic model (Figure 4.2 (b)), for each 0.1 m change in the wave's height, there would be a 50 μV change in the output voltage, meaning that by substituting the output voltage in the following equation, the wave's height can be measured:

$$H \approx \frac{V_{out}}{5\times10^{-4}}, \tag{6.1}$$

where H and V_{out} are the wave's height and the maximum output voltage, respectively.

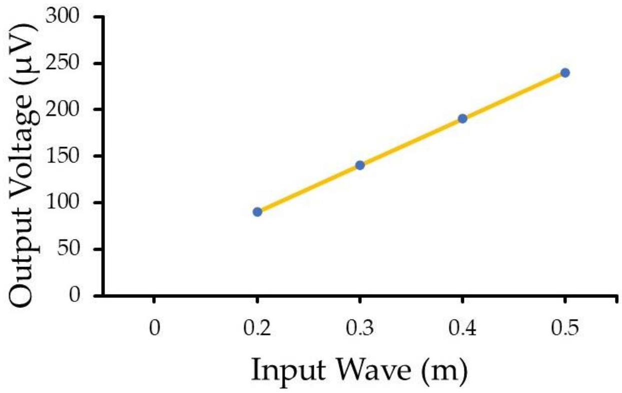

Figure 6. 1. Linear Relationship Between the Output Voltage and the Input Ocean Waves.

6.2 Comparison of Results

To compare the results of the dynamic model, FEA simulation, and the experimental results, their outputs are plotted in Figure 6.2. These results are for input waves of 0.2 m (Figure 6.2 (a)) and 0.3 m (Figure 6.2 (b)) heights with a 3.5 second period. Moreover, Table 2 lists and compares the peak values of output voltages in the simulations and the experiment.

Table 6. 1. Comparison of the Results.

		0.2 m	**0.3 m**	**0.4 m**	**0.5 m**
Results	Dynamic Model	90μV	140μV	190μV	240μV
	FEA	95μV	160μV	205μV	260μV
	Experiment	92μV	155μV	-	-
Error (%)	Dynamic and FEA	5.5	14.2	7.8	8.3
	Dynamic and Experiment	2.2	10	-	-
	FEA and Experiment	3.2	3.2	-	-

(a)

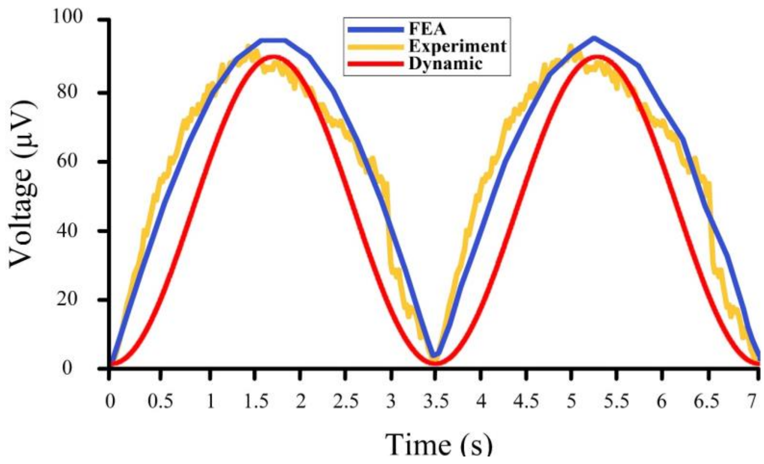

(b)

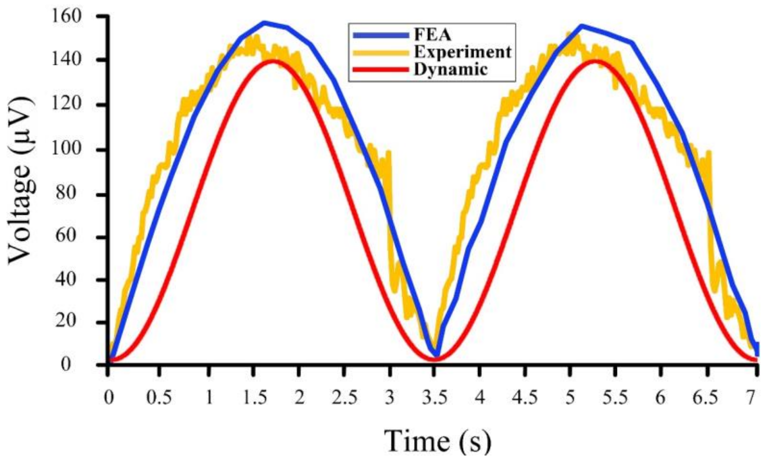

Figure 6. 2. Comparison of the Results of the Dynamic Model (Red Line), FEA Simulation (Blue Line), and the Experiment (Orange Line): (a) Results for 0.2 m Wave Height; and (b) Results for 0.3 m Wave Height.

As can be seen in Table 2, the average errors between the results are about 8%, which further verifies the feasibility of the proposed drifter-based piezoelectric sensor for oceanic wave measurement. There are also noises seen in the results of the experimental testing compared to the other two models, which are mainly caused by the coarse and non-linear motion of the slider-crank mechanism. Moreover, to further compare the results of the dynamic model and the FEA simulation, their outputs are plotted in Figure 6.3.

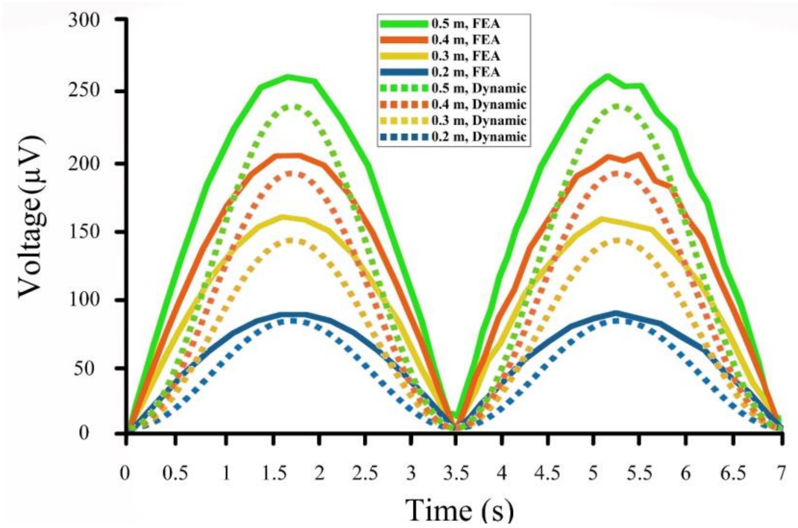

Figure 6. 3. Results of the Dynamic Model (Dashed Lines) and the FEA Simulation (Lines)

6.3 Sensor Resolution

The sensor's resolution, which is here the smallest ocean wave that can be measured, plays an important role in its selection for an application. Therefore, a set of analyses based on the proposed dynamic model in Chapter 4, is designed to realize the resolution of the proposed sensor. To do so, three types of input waves are applied to the sensor to see whether it can distinguish between them or not. The input waves have a difference of 0.05 m, 0.025 m, and 0.01 m in each set of the inputs:

1) 0.2 m, 0.25 m, 0.3 m, and 0.35 m for the first set;
2) 0.2 m, 0.225 m, 0.25 m, 0.275 m, and 0.3 m for the second set; and
3) 0.2 m, 0.21 m, 0.22 m, 0.23 m, 0.24 m, and 0.25 m for the third set.

Based on the output voltages for the designed sets of input waves, the sensor can successfully distinguish input waves with a difference of 0.05 m and 0.025 m in height, and a linear relationship is seen in Figure 6.4. However, the output voltages for input waves with a 0.01 m difference are not linear, thus the proposed sensor can only measure the ocean waves with more than 0.025 m in height.

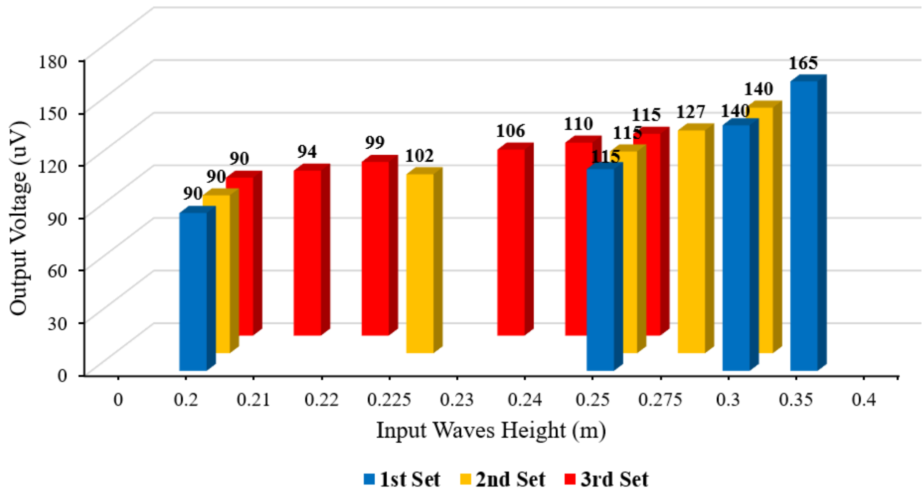

Figure 6. 4. Resolution Testing of the Sensor Based on the Proposed Dynamic Model.

6.4 Self-Powering Functionality

The proposed piezoelectric sensor aims to store the generated electricity in response to the ocean waves for further use to send the extracted data to a nearby station. In this regard, the sensor itself can be considered a piezoelectric energy harvester, which is a well-known subject of research in recent oceanic research [47]. In the case of the present sensor, as the generation of the output voltage is demonstrated in Chapters 4 and 5 using dynamic modeling, FEA simulation, and experimental testing, there would be an output power that can be stored in a battery [73]:

$$P = \frac{1}{T}\int_0^T \frac{V^2}{R} dt, \tag{6.2}$$

where P, R, V, and T are power, resistance, voltage, and period of V, respectively. It should be noted that, based on Equation (6.2), although the generated power by the present configuration is very low (nW-μW) and should be improved to power the sensor in a real environment independently, it can prove the sensor's self-powering functionality.

The battery as the power storage system of the sensor requires further processing of the generated electricity by the piezoelectric material: Batteries require direct current (DC), and the piezoelectric energy harvester generates alternative current (AC), which should be rectified before being stored in the battery. Therefore, adding an intermediate step to the circuit of the harvester would convert AC signals to DC [47]. Figure 6.5 shows the circuit of the energy harvester in the proposed piezoelectric sensor.

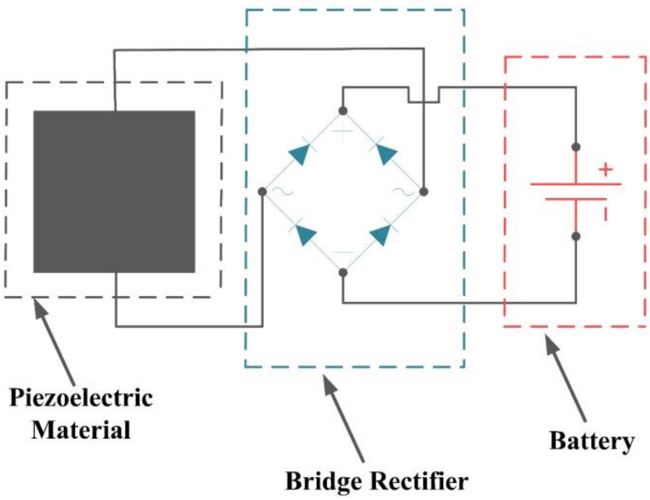

Figure 6. 5. Circuit of the Energy Harvester to Store the Generated Electricity in a Battery.

It should be noted that as the output voltage is low, the generated output power has some uncertainty, which requires a stable and well-calibrated electromechanical coupling coefficient for the material.

6.5 Summary

This Chapter has focused on providing insightful discussions on the proposed sensor's outputs. These discussions include:

1) Interpretation of the output voltages and converting them to wave height, for which an equation is provided to convert the output voltages to ocean waves' height. However, it should be noted that in reality, this will be more of a best fit to the line and not this close to the exact value;
2) Comparison of the outputs of the dynamic model, FEA simulation, and experimental testing, in which for an input wave of 0.2 m, 0.3 m, 0.4 m, and 0.5 m in height and 3.5 s in period, the calculated output voltages using the dynamic model are 90 μV, 140 μV, 190 μV, and 240 μV, respectively, whereas the output voltages of the FEA simulations are 95 μV, 160 μV, 205 μV, and 260 μV for the same input waves. Also, peak voltage values of 92 μV and 155 μV for waves with a height of 0.2 m and 0.3 m, respectively, are recorded using the experimental setup.
3) The sensor's resolution, which is demonstrated that it can only measure ocean waves with more than 0.025 m in height; and
4) Self-powering functionality that is demonstrated by a generic equation and is in the range of nW-μW. Moreover, the related circuit for self-powering functionality is provided.

7. Conclusions and Future Work

7.1 Conclusions

In this research, to measure ocean waves' height and period, a novel drifter-based piezoelectric sensor has been proposed, which is capable of being self-powered.

A dynamic model (mass-spring-damper system), based on Newton's second law of motion has been developed to analyze the proposed sensor's working performance and motion principle. For an input wave of 0.2 m, 0.3 m, 0.4 m, and 0.5 m in height and 3.5 seconds in period, the calculated output voltages using the dynamic model are 90 μV, 140 μV, 190 μV, and 240 μV, respectively. Furthermore, the effect of different parameters, such as mass and stiffness, of both the piezoelectric material and the drifter, and the period of the input waves on the output performance of the sensor is investigated: It is found that the period of the input waves is the same as the output voltages. Moreover, the lower stiffness of the piezoelectric material and the drifter result in a more readable output for interpretation and a higher output voltage, respectively. Furthermore, the mass of the piezoelectric material has a linear relationship to the output voltage.

To verify the results of the dynamic model, an FEA simulation using COMSOL-Multiphysics has been performed. Both Solid Mechanics and Electrostatics Modules are employed to develop a coupled-physics simulation for the proposed sensor. The output voltages of the FEA simulations are 95 μV, 160 μV, 205 μV, and 260 μV for the same input waves of the dynamic model.

To validate the results of the dynamic model and the FEA simulation, a prototype has been fabricated and tested. The peak voltage values of 92 μV and 155 μV have been recorded for waves with a height of 0.2 m and 0.3 m, respectively.

The results of the experimental testing show a close match with the results of the proposed dynamic model and FEA simulation. The average error between the results is about 8%, which further verifies the feasibility of the proposed piezoelectric sensor.

Through analyses based on the developed dynamic model, the resolution of the sensor is calculated, and the sensor is suitable for measuring oceanic waves of at least 0.025 m in height.

Finally, energy harvesting functionality, which leads to becoming self-powered, is discussed and demonstrated.

7.2 Future Work

This research was a preliminary study for using the output of the piezoelectric materials for sensory applications in the oceans. Therefore, several items should be addressed in our future work:

The fabricated prototype in this research was a preliminary prototype to verify the idea of developing self-powered piezoelectric sensors for ocean measurements. Therefore, a new prototype should be fabricated and tested in a real environment (the ocean).

The sensor needs to automatically interpret the outputs and send them to a station. This means that algorithms should be developed to train the sensor for autonomous purposes.

The other important issue that should be addressed in future research is the interpretation of the outputs for complex output voltages. To do so, some advanced mathematics can be used to interpret the results for complex input waves that are frequent in real environments.

To send the recorded data to a station, a low-power unit should be employed. The communication range of this unit and its power requirements are the most important factors in its selection for this sensor.

As it is discussed, the output power of the sensor (self-powering functionality) is very small. In our future work, by further optimizing the design and material parameters of the sensor, the output power should be enhanced to finally be able to fully power the sensor.

Design experiments to realize the expected range of operation for the sensor: Below a certain value, the noises dominate the output of the sensor, so the sensor will not be able to measure them. Moreover, higher accelerations can harm the piezoelectric material's performance. Therefore, there is also a maximum wave height for the sensor for precise measurement.

There are factors such as temperature fluctuations in oceans, maximum vibrational working cycles, etc., which influence the working performance of the piezoelectric material in long-term applications that need to be investigated in future work.

To enhance the sensitivity of the sensor, a seismic mass can be attached to it, which will be considered in our future research.

8. References

1. Young, A.M., et al., *An Unsteady Pressure Probe for the Measurement of Flow Unsteadiness in Tidal Channels.* IEEE Journal of Oceanic Engineering, 2020. **45**(4): p. 1411-1426.
2. Rossi, G.B., et al., *Measurement of Sea Waves.* Sensors, 2022. **22**(1).
3. Curie, P. and J. Curie, *Développement par compression de l'électricité polaire dans les cristaux hémièdres à faces inclinées.* Bulletin de Minéralogie, 1880: p. 90-93.
4. Jbaily, A. and R.W. Yeung, *Piezoelectric devices for ocean energy: a brief survey.* Journal of Ocean Engineering and Marine Energy, 2015. **1**(1): p. 101-118.
5. Shirinov, A.V. and W.K. Schomburg, *Pressure sensor from a PVDF film.* Sensors and Actuators A: Physical, 2008. **142**(1): p. 48-55.
6. Akitegetse, C., C. Volat, and M. Farzaneh, *Measuring bending stress on an ice/aluminium composite beam interface using an embedded piezoelectric PVDF (polyvinylidene-fluoride) film sensor.* Measurement Science and Technology, 2008. **19**(6): p. 065703.
7. Zhu, M., et al., *Piezoelectric polymer nanofibers for pressure sensors and their applications in human activity monitoring.* RSC Advances, 2020. **10**(37): p. 21887-21894.
8. Wang, Q.-M., et al., *Analysis of thin film piezoelectric microaccelerometer using analytical and finite element modeling.* Sensors and Actuators A: Physical, 2004. **113**(1): p. 1-11.
9. Crescini, D., et al., *Large bandwidth and thermal compensated piezoelectric thick-film acceleration transducer.* Sensors and Actuators A: Physical, 2001. **87**(3): p. 131-138.
10. Daku, B.L.F., E.M.A. Mohamed, and A.F. Prugger, *A PVDF transducer for low-frequency acceleration measurements.* ISA Transactions, 2004. **43**(3): p. 319-328.
11. Tseng, H.-J., W.-C. Tian, and W.-J. Wu, *Flexible PZT Thin Film Tactile Sensor for Biomedical Monitoring.* Sensors, 2013. **13**(5).
12. Fiorillo, A.S., P. Dario, and M. Bergamasco, *A sensorized robot gripper.* Robotics and Autonomous Systems, 1988. **4**(1): p. 49-55.
13. Justino, C.I.L., A.C. Duarte, and T.A.P. Rocha-Santos, *Chapter Three - Immunosensors in Clinical Laboratory Diagnostics*, in *Advances in Clinical Chemistry*, G.S. Makowski, Editor. 2016, Elsevier. p. 65-108.
14. Narita, F., et al., *A Review of Piezoelectric and Magnetostrictive Biosensor Materials for Detection of COVID-19 and Other Viruses.* Advanced Materials, 2021. **33**(1): p. 2005448.
15. Svečko, R., et al., *Acoustic Emission Detection of Macro-Cracks on Engraving Tool Steel Inserts during the Injection Molding Cycle Using PZT Sensors.* Sensors, 2013. **13**(5).

16. Aabid, A., et al., *A Review of Piezoelectric Material-Based Structural Control and Health Monitoring Techniques for Engineering Structures: Challenges and Opportunities.* Actuators, 2021. **10**(5).
17. Moure, A., et al., *Feasible integration in asphalt of piezoelectric cymbals for vibration energy harvesting.* Energy Conversion and Management, 2016. **112**: p. 246-253.
18. Deng, W., et al., *Cowpea-structured PVDF/ZnO nanofibers based flexible self-powered piezoelectric bending motion sensor towards remote control of gestures.* Nano Energy, 2019. **55**: p. 516-525.
19. Huang, P., et al., *Postcapture robust nonlinear control for tethered space robot with constraints on actuator and velocity of space tether.* International Journal of Robust and Nonlinear Control, 2017. **27**(16): p. 2824-2841.
20. Orrego, S., et al., *Harvesting ambient wind energy with an inverted piezoelectric flag.* Applied Energy, 2017. **194**: p. 212-222.
21. Nabavi, S.F., et al., *An ocean wave-based piezoelectric energy harvesting system using breaking wave force.* International Journal of Mechanical Sciences, 2019. **151**: p. 498-507.
22. Zhang, H., et al., *A flexible and implantable piezoelectric generator harvesting energy from the pulsation of ascending aorta: in vitro and in vivo studies.* Nano Energy, 2015. **12**: p. 296-304.
23. Gong, Y., et al., *Capturing Flow Energy from Ocean and Wind.* Energies, 2019. **12**(11).
24. Sezer, N. and M. Koç, *A comprehensive review on the state-of-the-art of piezoelectric energy harvesting.* Nano Energy, 2021. **80**: p. 105567.
25. Priya, S., *Advances in energy harvesting using low profile piezoelectric transducers.* Journal of Electroceramics, 2007. **19**(1): p. 167-184.
26. Jiang, B., et al., *Performance analysis and tank test validation of a hybrid ocean wave-current energy converter with a single power takeoff.* Energy Conversion and Management, 2020. **224**: p. 113268.
27. Anton, S.R. and H.A. Sodano, *A review of power harvesting using piezoelectric materials (2003–2006).* Smart Materials and Structures, 2007. **16**(3): p. R1-R21.
28. Kim, H.-M., *Electroactive polymers for ocean kinetic energy harvesting: literature review and research needs.* Journal of Ocean Engineering and Marine Energy, 2018. **4**(4): p. 343-365.
29. Kiran, M.R., et al., *Progress in Piezoelectric Material Based Oceanic Wave Energy Conversion Technology.* IEEE Access, 2020. **8**: p. 146428-146449.
30. Liu, H., et al., *A comprehensive review on piezoelectric energy harvesting technology: Materials, mechanisms, and applications.* Applied Physics Reviews, 2018. **5**(4): p. 041306.
31. Aabid, A., et al., *A Systematic Review of Piezoelectric Materials and Energy Harvesters for Industrial Applications.* Sensors, 2021. **21**(12).

32. Covaci, C. and A. Gontean, *Piezoelectric Energy Harvesting Solutions: A Review.* Sensors, 2020. **20**(12).
33. Mishra, S., et al., *Advances in Piezoelectric Polymer Composites for Energy Harvesting Applications: A Systematic Review.* Macromolecular Materials and Engineering, 2019. **304**(1): p. 1800463.
34. Mustapa, M.A., et al., *Wave energy device and breakwater integration: A review.* Renewable and Sustainable Energy Reviews, 2017. **77**: p. 43-58.
35. López, I., et al., *Review of wave energy technologies and the necessary power-equipment.* Renewable and Sustainable Energy Reviews, 2013. **27**: p. 413-434.
36. Yeung, R., *Fluid Dynamics of Finned Bodies – From VIV to FPSO.* Proceedings of the International Offshore and Polar Engineering Conference, 2002. **12**.
37. Akcabay, D. and Y.L. Young, *Hydroelastic response and energy harvesting potential of flexible piezoelectric beams in viscous flow.* Physics of Fluids, 2012. **24**.
38. Akimoto, H., K. Tanaka, and Y.Y. Kim, *Drag-type cross-flow water turbine for capturing energy from the orbital fluid motion in ocean wave.* Renewable Energy, 2015. **76**: p. 196-203.
39. Athanassoulis, G.A. and K.I. Mamis, *Modeling and analysis of a cliff-mounted piezoelectric sea-wave energy absorption system.* Coupled systems mechanics, 2013. **2**(1): p. 53-83.
40. Ton, A., et al., *27 - Beach and nearshore monitoring techniques*, in *Sandy Beach Morphodynamics*, D.W.T. Jackson and A.D. Short, Editors. 2020, Elsevier. p. 659-687.
41. Subbaraya, S., et al., *Circling the Seas: Design of Lagrangian Drifters for Ocean Monitoring.* IEEE Robotics & Automation Magazine, 2016. **23**: p. 1-1.
42. Carandell, M., et al., *Design and Testing of a Kinetic Energy Harvester Embedded Into an Oceanic Drifter.* IEEE Sensors Journal, 2020. **20**(23): p. 13930-13939.
43. Toffoli, A. and E.M. Bitner-Gregersen, *Types of Ocean Surface Waves, Wave Classification.* Encyclopedia of Maritime and Offshore Engineering, 2017: p. 1-8.
44. Guillou, N., *Estimating wave energy flux from significant wave height and peak period.* Renewable Energy, 2020. **155**: p. 1383-1393.
45. Farrok, O., et al., *Electrical Power Generation from the Oceanic Wave for Sustainable Advancement in Renewable Energy Technologies.* Sustainability, 2020. **12**(6).
46. Viet, N.V., N. Wu, and Q. Wang, *A review on energy harvesting from ocean waves by piezoelectric technology.* Journal of Modeling in Mechanics and Materials, 2017. **1**(2).

47. Kargar, S.M. and G. Hao, *An Atlas of Piezoelectric Energy Harvesters in Oceanic Applications.* Sensors, 2022. **22**(5).
48. Liang, H., G. Hao, and O.Z. Olszewski, *A review on vibration-based piezoelectric energy harvesting from the aspect of compliant mechanisms.* Sensors and Actuators A: Physical, 2021. **331**: p. 112743.
49. Centurioni, L., et al., *A Global Ocean Observing System for Measuring Sea Level Atmospheric Pressure: Effects and Impacts on Numerical Weather Prediction.* Bulletin of the American Meteorological Society, 2017. **98**(2): p. 231-238.
50. Lumpkin, R. and M. Pazos, *Lagrangian Analysis and Prediction in Coastal and Ocean Processes, chap. Measuring surface currents with Surface Velocity Program drifters: the instrument, its data, and some recent results.* Cambridge University Press, https://doi. org/10.1017/CBO9780511535901, 2007. **3**: p. 39-67.
51. Centurioni, L., et al., *A new strategic wave measurement station off Naples port main breakwater.* Coast. Eng. Proc, 2017. **1**: p. 36.
52. Liao, Z., et al., *Snow depth and ice thickness derived from SIMBA ice mass balance buoy data using an automated algorithm.* International Journal of Digital Earth, 2019. **12**(8): p. 962-979.
53. Ulaby, F.T., *Microwave remote sensing active and passive.* Rader remote sensing and surface scattering and emission theory, 1982: p. 848-902.
54. Barrick, D. *Remote sensing of sea state by radar*. IEEE.
55. Barrick, D.E., *Extraction of wave parameters from measured HF radar sea-echo Doppler spectra.* Radio Science, 1977. **12**(3): p. 415-424.
56. Ardhuin, F., L. Gualtieri, and E. Stutzmann, *How ocean waves rock the Earth: Two mechanisms explain microseisms with periods 3 to 300 s.* Geophysical Research Letters, 2015. **42**(3): p. 765-772.
57. Ardhuin, F., et al., *From seismic noise to ocean wave parameters: General methods and validation.* Journal of Geophysical Research: Oceans, 2012. **117**(C5).
58. Bromirski, P.D., F.K. Duennebier, and R.A. Stephen, *Mid-ocean microseisms.* Geochemistry, Geophysics, Geosystems, 2005. **6**(4).
59. Wyatt, L.R., J.J. Green, and A. Middleditch, *HF radar data quality requirements for wave measurement.* Coastal Engineering, 2011. **58**(4): p. 327-336.
60. Pratt, M.J., et al., *Implications of sea ice on Southern Ocean microseisms detected by a seismic array in West Antarctica.* Geophysical Journal International, 2017. **209**(1): p. 492-507.
61. Hausler, E. and L. Stein, *Hydromechanical and physiological mechanical-to-electrical power converter with PVDF film.* Ferroelectrics, 1987. **75**(1): p. 363-369.

62. Burns, J.R., *OCEAN WAVE ENERGY CONVERSION USING PIEZOELECTRIC MATERIAL MEMBERS*. 1987: The U.S., Patent Number: US4685296.
63. Taylor, G.W., et al., *The Energy Harvesting Eel: a small subsurface ocean/river power generator.* IEEE Journal of Oceanic Engineering, 2001. **26**(4): p. 539-547.
64. Pobering, S. and N. Schwesinger. *A Novel Hydropower Harvesting Device*. in *2004 International Conference on MEMS, NANO and Smart Systems (ICMENS'04)*. 2004.
65. Zurkinden, A.S., F.C. Campanile, and L. Martinelli. *Wave Energy Converter through Piezoelectric Polymers*. 2007.
66. Murray, R. and J. Rastegar. *Novel two-stage piezoelectric-based ocean wave energy harvesters for moored or unmoored buoys*. in *Proc.SPIE*. 2009.
67. Mutsuda, H., et al., *A Technology of Electrical Energy Generated From Ocean Power Using Flexible Piezoelectric Device*, in *ASME 2010 29th International Conference on Ocean, Offshore and Arctic Engineering*. 2010. p. 313-321.
68. Mutsuda, H., et al., *Study on Wave Power Generator Using Flexible Piezoelectric Device*, in *ASME 2011 30th International Conference on Ocean, Offshore and Arctic Engineering*. 2011. p. 267-273.
69. Mutsuda, H., et al., *Elastic Floating Unit With Piezoelectric Device for Harvesting Ocean Wave Energy*, in *ASME 2012 31st International Conference on Ocean, Offshore and Arctic Engineering*. 2012. p. 233-240.
70. Mutsuda, H., et al., *Ocean Power Generator Using Flexible Piezoelectric Device*, in *ASME 2013 32nd International Conference on Ocean, Offshore and Arctic Engineering*. 2013.
71. Molino-Minero-Re, E., et al. *Piezoelectric energy harvesting from induced vortex in water flow*. in *2012 IEEE International Instrumentation and Measurement Technology Conference Proceedings*. 2012.
72. Okada, N., et al., *Experiments on floating wave-power generation using piezoelectric elements and pendulums in the water tank.* 2012 Oceans - Yeosu, 2012: p. 1-8.
73. Kim, K.-B., et al., *Energy Harvesting Characteristics from Water Flow by Piezoelectric Energy Harvester Device Using Cr/Nb Doped Pb(Zr,Ti)O3Bimorph Cantilever.* Japanese Journal of Applied Physics, 2013. **52**(10S): p. 10MB01.
74. Xie, X.D., Q. Wang, and N. Wu, *Potential of a piezoelectric energy harvester from sea waves.* Journal of Sound and Vibration, 2014. **333**(5): p. 1421-1429.
75. Xie, X.D., Q. Wang, and N. Wu, *Energy harvesting from transverse ocean waves by a piezoelectric plate.* International Journal of Engineering Science, 2014. **81**(Complete): p. 41-48.

76. Woo, M.S., et al., *Relationship between current and impedance in piezoelectric energy harvesting system for water waves.* Journal of Electroceramics, 2015. **34**(2): p. 180-184.
77. Gao, X., et al. *A study of piezoelectric generator based on the flow around a blunt body*. in *2014 17th International Conference on Electrical Machines and Systems (ICEMS)*. 2014.
78. Song, R., et al., *A Novel Piezoelectric Energy Harvester Using the Macro Fiber Composite Cantilever with a Bicylinder in Water.* Applied Sciences, 2015. **5**(4).
79. Song, R., et al., *A study of vortex-induced energy harvesting from water using PZT piezoelectric cantilever with cylindrical extension.* Ceramics International, 2015. **41**(Supplement 1): p. S768-S773.
80. Sarker, M.R., A. Mohamed, and R. Mohamed. *Cantilever beam vibration from fluid interactions with triangular shape blunt body for energy harvesting application*. in *2015 IEEE Student Conference on Research and Development (SCOReD)*. 2015.
81. Feifei, P., et al. *Designed simulation and experiment of a piezoelectric energy harvesting system based on flow around blunt bodies*. in *2015 18th International Conference on Electrical Machines and Systems (ICEMS)*. 2015.
82. Shan, X., et al., *Novel energy harvesting: A macro fiber composite piezoelectric energy harvester in the water vortex.* Ceramics International, 2015. **41**: p. S763-S767.
83. Wu, N., Q. Wang, and X. Xie, *Ocean wave energy harvesting with a piezoelectric coupled buoy structure.* Applied Ocean Research, 2015. **50**: p. 110-118.
84. Toma, D.M., et al. *Underwater energy harvesting system based on plucked-driven piezoelectrics*. in *OCEANS 2015 - Genova*. 2015.
85. Cha, Y., et al., *Energy harvesting from a piezoelectric biomimetic fish tail.* Renewable Energy, 2016. **86**: p. 449-458.
86. Li, H., et al., *An Energy Harvesting Underwater Acoustic Transmitter for Aquatic Animals.* Scientific Reports, 2016. **6**(1): p. 33804.
87. Viet, N.V., et al., *Energy harvesting from ocean waves by a floating energy harvester.* Energy, 2016. **112**: p. 1219-1226.
88. Kamenar, E., et al., *Harvesting of river flow energy for wireless sensor network technology.* Microsystem Technologies, 2016. **22**(7): p. 1557-1574.
89. Renzi, E., *Hydroelectromechanical modelling of a piezoelectric wave energy converter.* Proceedings of the Royal Society A: Mathematical, Physical and Engineering Sciences, 2016. **472**(2195): p. 20160715.
90. Mutsuda, H., et al., *A painting type of flexible piezoelectric device for ocean energy harvesting.* Applied Ocean Research, 2017. **68**: p. 182-193.

91. Shan, X., et al., *A Piezoelectric Energy Harvester with Bending–Torsion Vibration in Low-Speed Water.* Applied Sciences, 2017. **7**(2).
92. Xie, X.D. and Q. Wang, *A study on an ocean wave energy harvester made of a composite piezoelectric buoy structure.* Composite Structures, 2017. **178**: p. 447-454.
93. Hwang, W.S., et al., *Design of piezoelectric ocean-wave energy harvester using sway movement.* Sensors and Actuators A: Physical, 2017. **260**: p. 191-197.
94. Viet, N.V., Q. Wang, and A. Carpinteri, *Development of an ocean wave energy harvester with a built-in frequency conversion function.* International Journal of Energy Research, 2018. **42**(2): p. 684-695.
95. An, X., et al. *Numerical simulation of Vortex Induced Piezoelectric Energy Converter (VIPEC) based on coupled fluid, structure and piezoelectric interaction*. in *OCEANS 2017 - Aberdeen*. 2017.
96. An, X., et al., *Design and CFD Simulations of a Vortex-Induced Piezoelectric Energy Converter (VIPEC) for Underwater Environment.* Energies, 2018. **11**(2).
97. Dessi, D., G. Leonardi, and F. Passacantilli, *Energy Harvesting From Waves Using Piezoelectric Floaters*, in *ASME 2018 37th International Conference on Ocean, Offshore and Arctic Engineering*. 2018.
98. Nabavi, S.F., A. Farshidianfar, and A. Afsharfard, *Novel piezoelectric-based ocean wave energy harvesting from offshore buoys.* Applied Ocean Research, 2018. **76**: p. 174-183.
99. Nguyen, V. and Q. Wang, *Ocean Wave Energy Pitching Harvester with a Frequency Tuning Capability.* Energy, 2018. **162**.
100. Salazar, R., et al., *Optimal design and energy harvesting performance of carangiform fish-like robotic system.* Smart Materials and Structures, 2018. **27**(7): p. 075045.
101. Aramendia, I., et al., *Power Control Optimization of an Underwater Piezoelectric Energy Harvester.* Applied Sciences, 2018. **8**(3).
102. Ming, L., et al., *Performance Analysis for a Wave Energy Harvester of Piezoelectric Cantilever Beam.* Journal of Coastal Research, 2019. **83**(sp1): p. 976-984.
103. Gong, Y., et al., *270-degree arc-shaped piezoelectric energy converter in uniflow fluid environment.* IOP Conference Series: Materials Science and Engineering, 2019. **531**: p. 012026.
104. Viet, N.V., A. Carpinteri, and Q. Wang, *A Novel Heaving Ocean Wave Energy Harvester with a Frequency Tuning Capability.* Arabian Journal for Science and Engineering, 2019. **44**(6): p. 5711-5722.
105. Bao, B., W. Chen, and Q. Wang, *A piezoelectric hydro-energy harvester featuring a special container structure.* Energy, 2019. **189**: p. 116261.

106. Zhang, J., et al., *A study on a near-shore cantilevered sea wave energy harvester with a variable cross section.* Energy Science & Engineering, 2019. **7**(6): p. 3174-3185.
107. Mutsuda, H., et al., *Application of a flexible device coating with piezoelectric paint for harvesting wave energy.* Ocean Engineering, 2019. **172**: p. 170-182.
108. Gong, Y., et al., *Direction-adaptive energy harvesting with a guide wing under flow-induced oscillations.* Energy, 2019. **187**: p. 115983.
109. Sun, W., et al., *Low velocity water flow energy harvesting using vortex induced vibration and galloping.* Applied Energy, 2019. **251**: p. 113392.
110. Shan, X., et al., *Enhancing the performance of an underwater piezoelectric energy harvester based on flow-induced vibration.* 2019-04-01. **v. 172**.
111. Noh, H.-J., J.-S. Lee, and Y.-J. Kim, *Micro-energy harvesting based on vortex-induced vibration of cross-flow hydroturbine with various cantilever beam configurations.* IOP Conference Series: Earth and Environmental Science, 2019. **240**: p. 022034.
112. Liu, H.-x., et al., *Piezoelectric Energy Analysis on Diverse Buoy Coupling with Hydrodynamic Parameters.* China Ocean Engineering, 2019. **33**(3): p. 279-287.
113. Yayla, S., S. Ayça, and M. Oruç, *A case study on piezoelectric energy harvesting with using vortex generator plate modeling for fluids.* Renewable Energy, 2020. **157**: p. 1243-1253.
114. Cao, D., et al., *Design, Simulation and Experiment for a Vortex-Induced Vibration Energy Harvester for Low-Velocity Water Flow.* International Journal of Precision Engineering and Manufacturing-Green Technology, 2021. **8**(4): p. 1239-1252.
115. Shan, X., H. Tian, and T. Xie, *Enhanced performance of piezoelectric energy harvester through three serial vibrators.* Journal of Intelligent Material Systems and Structures, 2020. **32**(10): p. 1140-1151.
116. Du, X., et al., *Enhancement of the Piezoelectric Cantilever Beam Performance via Vortex-Induced Vibration to Harvest Ocean Wave Energy.* Shock and Vibration, 2020. **2020**: p. 8858529.
117. Latif, U., et al., *Experimental investigation of energy harvesting eel in the wake of bluff body under ocean waves.* Proceedings of the Institution of Mechanical Engineers, Part M: Journal of Engineering for the Maritime Environment, 2020. **235**(1): p. 81-92.
118. Kim, S., et al., *Propeller-based Underwater Piezoelectric Energy Harvesting System for an Autonomous IoT Sensor System.* Journal of the Korean Physical Society, 2020. **76**(3): p. 251-256.
119. Qi, L., et al., *A hybrid piezoelectric-electromagnetic wave energy harvester based on capsule structure for self-powered applications in sea-crossing bridges.* Renewable Energy, 2021. **178**: p. 1223-1235.

120. Bao, B. and Q. Wang, *Bladeless rotational piezoelectric energy harvester for hydroelectric applications of ultra-low and wide-range flow rates.* Energy Conversion and Management, 2021. **227**: p. 113619.
121. Kazemi, S., et al., *Energy harvesting from longitudinal and transverse motions of sea waves particles using a new waterproof piezoelectric waves energy harvester.* Renewable Energy, 2021. **179**: p. 528-536.
122. Zhao, D., et al., *Hydrokinetic piezoelectric energy harvesting by wake induced vibration.* Energy, 2021. **220**: p. 119722.
123. Jiao, P., et al., *Mechanical Metamaterials Gyro-Structure Piezoelectric Nanogenerators for Energy Harvesting under Quasi-Static Excitations in Ocean Engineering.* ACS Omega, 2021. **6**(23): p. 15348-15360.
124. Song, R., et al., *Modeling, Validation, and Performance of Two Tandem Cylinder Piezoelectric Energy Harvesters in Water Flow.* Micromachines, 2021. **12**(8).
125. Mariello, M., et al., *Multifunctional sub-100 µm thickness flexible piezo/triboelectric hybrid water energy harvester based on biocompatible AlN and soft parylene C-PDMS-Ecoflex™.* Nano Energy, 2021. **83**: p. 105811.
126. Ucar, H., *Patch-based piezoelectric energy harvesting on a marine boat exposed to wave-induced loads.* Ocean Engineering, 2021. **236**: p. 109568.
127. Zheng, S., et al., *Performance of a plate-wave energy converter integrated in a floating breakwater.* IET Renewable Power Generation, 2021. **n/a**(n/a).
128. Salazar, R., R. Quintana, and A. Abdelkefi, *Role of Electromechanical Coupling, Locomotion Type and Damping on the Effectiveness of Fish-Like Robot Energy Harvesters.* Energies, 2021. **14**(3).
129. Yulianti, S., P. Kevin, and A. Prakoso, *The Use of Piezoelectric as Energy Harvester in Breakwater.* IOP Conference Series: Earth and Environmental Science, 2021. **750**(1): p. 012016.
130. Du, X., et al., *Theoretical study on a novel piezoelectric ocean wave energy harvester driven by oscillating water column.* Energy Sources, Part A: Recovery, Utilization, and Environmental Effects, 2021: p. 1-21.
131. Alizzio, D., et al., *Design and Performance Evaluation of a "Fixed-Point" Spar Buoy Equipped with a Piezoelectric Energy Harvesting Unit for Floating Near-Shore Applications.* Sensors, 2021. **21**(5).
132. Tan, D., et al., *Trout-like multifunctional piezoelectric robotic fish and energy harvester.* Bioinspiration & Biomimetics, 2021. **16**(4): p. 046024.
133. Wang, D.A. and H.H. Ko, *Piezoelectric energy harvesting from flow-induced vibration.* Journal of Micromechanics and Microengineering Structures, Devices and Systems, 2010. **20**(2): p. 9.
134. Wang, D.-A. and N.-Z. Liu, *A shear mode piezoelectric energy harvester based on a pressurized water flow.* Sensors and Actuators A: Physical, 2011. **167**(2): p. 449-458.
135. Toma, D.M., et al. *An impacting energy harvester through piezoelectric device for oscillating water flow*. 2013.

136. Viñolo, C., et al., *Sea motion electrical energy generator for low-power applications.* 2013 MTS/IEEE OCEANS - Bergen, 2013: p. 1-7.
137. Viñolo, C., et al., *An ocean kinetic energy converter for low-power applications using piezoelectric disk elements.* The European Physical Journal Special Topics, 2013. **222**(7): p. 1685-1698.
138. Abrol, S., D. Chhabra, and D. Chhabra, *Experimental Investigations of Piezoelectric Energy Harvesting with Turbulent Flow.* International Journal of Mechanical and Production Engineering Research and Development, 2018. **8**: p. 703-710.
139. Huang, W. and Y. Huang. *A Study on Piezoelectric Buoy Energy Harvester Based on Orthogonal Experimental Design*. in *2019 IEEE International Conference on Power, Intelligent Computing and Systems (ICPICS)*. 2019.
140. Zhang, B., et al., *Experimental sea wave energy extractor based on piezoelectric Ericsson cycles.* Journal of Intelligent Material Systems and Structures, 2017. **29**(6): p. 1102-1112.
141. Chen, S.-E., et al., *A Piezoelectric Wave-Energy Converter Equipped with a Geared-Linkage-Based Frequency Up-Conversion Mechanism.* Sensors, 2021. **21**(1).
142. Bezanson, L., et al., *Utilizing deep ocean currents to power extended duration sensors.* OCEANS 2010 MTS/IEEE SEATTLE, 2010: p. 1-8.
143. Zou, H.-X., et al., *A magnetically coupled bistable piezoelectric harvester for underwater energy harvesting.* Energy, 2021. **217**: p. 119429.
144. Ponamgi, S.R. and T. Hang-Sheng, *Theoretical Calculation of Capacitance of an IDT Over a Piezoelectric Layered Structure.* IEEE Transactions on Sonics and Ultrasonics, 1974. **21**(2): p. 125-127.
145. Zhou, Y. and M. Zaghloul, *Changes in Permittivity of the Piezoelectric Material PVDF as Functions of the Electrical Field and Temperature.* Materials (Basel, Switzerland), 2021. **14**(19): p. 5736.